



**HAL**  
open science

## Effect of fine particles on the hydraulic behavior of interlayer soil in railway substructure

Trong Vinh Duong, Yu-Jun Cui, Anh Minh A.M. Tang, Jean Claude Dupla,  
Nicolas Calon

► **To cite this version:**

Trong Vinh Duong, Yu-Jun Cui, Anh Minh A.M. Tang, Jean Claude Dupla, Nicolas Calon. Effect of fine particles on the hydraulic behavior of interlayer soil in railway substructure. Canadian Geotechnical Journal, 2014, 51 (7), pp.735-746. 10.1139/cgj-2013-0170 . hal-01111160

**HAL Id: hal-01111160**

**<https://enpc.hal.science/hal-01111160>**

Submitted on 25 Apr 2018

**HAL** is a multi-disciplinary open access archive for the deposit and dissemination of scientific research documents, whether they are published or not. The documents may come from teaching and research institutions in France or abroad, or from public or private research centers.

L'archive ouverte pluridisciplinaire **HAL**, est destinée au dépôt et à la diffusion de documents scientifiques de niveau recherche, publiés ou non, émanant des établissements d'enseignement et de recherche français ou étrangers, des laboratoires publics ou privés.

1 **Effect of fine particles on the hydraulic behavior of interlayer**  
2 **soil in railway substructure**

3 Trong Vinh DUONG<sup>1</sup>, Yu-Jun CUI<sup>1</sup>, Anh Minh TANG<sup>1</sup>, Jean-Claude DUPLA<sup>1</sup>, Nicolas  
4 CALON<sup>2</sup>

5 <sup>1</sup> *Ecole des Ponts Paris Tech (ENPC), Laboratoire Navier/CERMES*

6 <sup>2</sup> *French Railway Company (SNCF)*

7

8

9 **Corresponding author:**

10 Prof. Yu-Jun CUI

11 Ecole des Ponts ParisTech

12 6-8 av. Blaise Pascal, Cité Descartes, Champs-sur-Marne

13 F-77455 MARNE LA VALLEE - France

14 Telephone : +33 1 64 15 35 50

15 Fax : +33 1 64 15 35 62

16 E-mail : [yujun.cui@enpc.fr](mailto:yujun.cui@enpc.fr)

17 **Abstract:**

18 The ancient railway substructure in France was built by emplacing ballast directly on sub-grade.  
19 Over years of operation, the inter-penetration of ballast and sub-grade created a soil layer  
20 between them. Under different conditions, this naturally formed layer, namely interlayer, can  
21 contain different quantities of fine particles, becoming more or less sensitive to changes in water  
22 content. As the water content changes are governed by the hydraulic behavior of interlayer soil,  
23 assessing the influence of fine particles content on the hydraulic behavior of interlayer soil is  
24 important. To this end, the hydraulic behavior of an interlayer soil taken from Sénissiat (near  
25 Lyon, France) was investigated using two infiltration columns, a large-scale column equipped  
26 with tensiometers and TDR for suction and volumetric water content measurements, respectively,  
27 and a smaller column equipped with high capacity tensiometers only. Different fines contents  
28 were considered and wetting-drying cycles were applied to the soil specimens. The hydraulic  
29 conductivity was determined by applying the instantaneous profile method. The results obtained  
30 showed that i) hysteresis exists for both the soil water retention curve and the hydraulic  
31 conductivity changes with suction; ii) the effect of wetting-drying cycles is insignificant; iii)  
32 adding 10% of fine particles to the natural interlayer soil changes the soil water retention curve  
33 but does not induce significant changes in hydraulic conductivity; iv) the hydraulic conductivity  
34 of interlayer soil with 10% of fine particles added is close to that of soil sieved at 2 mm,  
35 suggesting that the hydraulic conductivity of interlayer soil is mainly governed by fine particles  
36 through suction effect.

37 **Keywords:** railway substructure; interlayer soil; fines content; instantaneous profiles method;  
38 hydraulic conductivity.

39

## 40 ***Introduction***

41 Many railway lines over the world have been in operation for more than one hundred years. In  
42 France, the ancient lines represent 94% of the whole railway network. As opposed to the new  
43 lines, the ancient ones were constructed by direct installation of ballast onto sub-grade without  
44 any separation layer. Over years of operation and with the increasing traffic, load, and speed of  
45 train, there are more and more problems related to the stability, loss of strength of substructure. A  
46 number of studies have been conducted to assess the state of substructure and to develop  
47 adequate maintenance methods (Trinh 2011; Duong et al. 2013; Cui et al. 2013). It was found  
48 that one of the particularities of ancient substructure is the presence of a soil layer namely  
49 interlayer that has been created mainly by interpenetration of ballast and fine particles of sub-  
50 grade.

51 In France, it has been decided recently to renew the ancient railway network. During the  
52 renewal, the interlayer will be kept as part of the substructure thanks to its high mechanical  
53 resistance related to its high dry unit mass ( $2.4 \text{ Mg/m}^3$  at the S nissiat site, according to Trinh et  
54 al. 2011) reached by natural dynamic compaction corresponding to the circulation of trains.  
55 However, the mechanical behavior of interlayer soil can show a large variability, depending on  
56 the proportion of fine particles contained in it. A number of studies (Babic et al. 2000; Pedro  
57 2004; Naeini and Baziar 2004; Kim et al. 2005; Verdugo and Hoz 2007; Cabalar 2008; Seif  
58 El Dine et al. 2010; Ebrahimi 2011; Anbazhagan et al. 2011; Trinh et al. 2012) showed that the  
59 mechanical behavior of soil containing a large proportion of fines is strongly influenced by the  
60 water content. As the water content changes are governed by the hydraulic behavior of soil, it  
61 appears important to assess the influence of fine particles content on the hydraulic behavior of  
62 interlayer soil.

63           Moreover, in field conditions, the interlayer soil normally undergoes the effect of  
64 wetting/drying cycles related to climatic changes. These wetting/drying cycles may induce  
65 changes in soil micro-structure, thereby changing the soil hydraulic properties. Therefore, it  
66 appears also important to investigate the effect of wetting/drying cycles on the hydraulic  
67 conductivity.

68           To the authors' knowledge, the effects of fines content and wetting/drying cycles on the  
69 unsaturated interlayer soil have not been investigated yet. In the present work, laboratory tests  
70 were performed using a large-scale infiltration column (300 mm in diameter) and a small-scale  
71 infiltration column (50 mm in diameter), and the instantaneous profile method was used to  
72 determine the hydraulic conductivity of soil. Both wetting and drying paths were performed and  
73 different fines contents were considered: natural interlayer soil ( $ITL_0$ ), natural interlayer soil with  
74 10% of sub-grade added ( $ITL_{10}$ ), fine-grained soil prepared by passing  $ITL_{10}$  through a 2 mm  
75 sieve (*Fines*). The results enable the assessment of the effects of fine particles and wetting/drying  
76 cycles.

## 77 ***Materials studied***

78           The soils (both the interlayer soil and sub-grade) were taken from the railway site S nissiat  
79 (North-West of Lyon, France). Mineralogy analysis reveals that the interlayer soil is a mixture of  
80 materials that come from the construction and maintenance (broken stones, gravel, sand, etc) of  
81 tracks, the aging process of track components and the sub-grade. It also showed that the fine  
82 particles in the interlayer soil mainly come from the sub-grade. The main geotechnical properties  
83 of interlayer soil and sub-grade are presented in Table 1. The results show that the sub-grade is  
84 high-plasticity silt. More details about the characterization of the interlayer soil can be found in  
85 Trinh et al. (2011).

86 In order to study the effect of fines contents on the hydraulic behavior of interlayer soil, a  
 87 quantity of sub-grade representing 10% of interlayer soil by dry mass was added into the  
 88 interlayer soil to form a soil with a higher content of fines:  $ITL_{10}$ . The grain size distribution  
 89 curves of the natural interlayer soil ( $ITL_0$ ) and  $ITL_{10}$  are presented in Fig. 1.

90 It is worth noting that the migration of fines into ballast is recognized as one of the  
 91 mechanisms for fouled ballast (Ayres 1986; Selig and Waters 1994; Alobaidi and Hoare 1996;  
 92 1998; Ghaotara et al. 2006; Mayoraz et al. 2006; Huang et al. 2009; Giannakos 2010; Fortunato  
 93 et al. 2010; Indraratna et al. 2011; Ebrahimi 2011; Sussmann and Chrismer 2012). Even though  
 94 the interlayer soil studied here is different from the fouled ballast by nature, in order to compare  
 95 with the classification of fouled ballast, two parameters for fouled ballast are adopted here: the  
 96 fouling index  $FI$  (Selig and Water 1994) and the relative fouling ratio  $R_{b-f}$  (Indraratna et al. 2011).  
 97  $FI$  is defined as:

98

99 [1] 
$$FI = P_4 + P_{200}$$

100 where  $P_4$  and  $P_{200}$  are percentages of ballast passing through sieves N° 4 (4.75 mm) and N° 200  
 101 (0.075 mm), respectively.

102  $R_{b-f}$  is the weighted ratio of the dry mass of fouling particles  $M_f$  (passing through 9.5 mm  
 103 sieve) to the dry mass of ballast  $M_b$  (particles retained in 9.5 mm sieve):

104 [2] 
$$R_{b-f} = \frac{M_f \times \frac{G_{s-b}}{G_{s-f}}}{M_b} \times 100\%$$

105 where  $G_{s-f}$ ,  $G_{s-b}$  are specific densities of fouling particles and ballast, respectively.

106 The values of the two indexes for  $ITL_0$  and  $ITL_{10}$  are presented in Table 2. According to  
107 the classification, both  $ITL_0$  and  $ITL_{10}$  are “highly fouled”. Because  $ITL_{10}$  is classified in the  
108 highest category of fouling, it was decided to not adding more fine particles to the interlayer soil.

109 To better evaluate the effect of fines on the hydraulic behavior of interlayer soil, the  
110 hydraulic conductivity of pure fine particles was also determined. For this purpose,  $ITL_{10}$  was  
111 sieved at 2 mm to obtain the fine part (namely *Fines*). The grain size distribution curve of *Fines*  
112 is also presented in Fig. 1.

### 113 ***Experimental methods***

114 The interlayer soil was tested in a large-scale infiltration column (Fig. 2). The column (300 mm  
115 in diameter and 600 mm in height) is equipped with five water content sensors (TDR1 to TDR5)  
116 and five tensiometers for measuring pore-water pressure (T1 to T5) arranged at various elevations  
117 along the column ( $h = 100, 200, 300, 400$  and  $500$  mm from the bottom of the soil specimen).  
118 The working pressure range of the tensiometers is from 100 kPa to -85 kPa. The accuracy of the  
119 TDR used is  $\pm 2\%$  and that of the tensiometer is  $\pm 0.5$  kPa. At each instrumented height, as the  
120 area occupied by the sensors is just 6.8% of the total apparatus section area, the influence of the  
121 sensors installation on water transfer is expected to be insignificant.

122 For the  $ITL_{10}$  specimen preparation, water and fine particles were added to the dry natural  
123 interlayer soil to reach the target water content and fine particles content, and a large mixer was  
124 used to homogenize the material. For the  $ITL_0$  specimen preparation, only desired quantity of  
125 water was added to the dry natural interlayer soil. After mixing, the wet materials were stored in  
126 hermetic containers for at least 24 h for moisture homogenization. Soil compaction was  
127 conducted using a vibrating hammer in six layers of 0.10 m each at a dry unit mass of 2.01

128  $\text{Mg/m}^3$ . The soil for each layer has a same composition as that of the whole sample. Big particles  
129 and fine particles were rearranged before the compaction in order to ensure the sample  
130 homogenization. Prior to the compaction of the subsequent layer, a TDR probe and a metal rod of  
131 25 mm diameter were placed on the compacted layer.

132         Once the soil specimen was prepared, water was injected from the bottom and it flowed  
133 out from the outlet after about half an hour. After saturation of the sample, the metal rods were  
134 removed and the tensiometers were installed. This protocol was adopted to avoid damaging the  
135 tensiometers during the compaction and also any cavitation due to possible high suction in the  
136 column. More details about the large-scale infiltration column can be found in Duong et al.  
137 (2013).

138         The TDR is an indirect measurement method and several authors reported that the  
139 calibration curve depends on the soil texture, unit mass, mineralogy, fines content and particle  
140 size (Jacobsen and Schjønning 1993; Stolte et al. 1994; Côté and Roy 1998; Gong et al. 2003;  
141 Schneider and Fratta 2009). It is therefore necessary to determine the specific calibration curve  
142 for each soil studied. For the natural interlayer soil ( $ITL_0$ ), a relationship between volumetric  
143 water content ( $\theta$ ) and the dielectric constant  $K_a$  was established by Duong et al. (2013). As the  
144 soil composition in  $ITL_{10}$  is different from  $ITL_0$ , another relationship was needed. This was  
145 determined separately with a lower specimen of 200 mm at the same unit mass in the same  
146 column. One TDR sensor was placed in the middle of the sample. Water was added on the  
147 surface of the soil specimen to achieve the desired water content. Once the TDR gave a steady  
148 response (after about 8 hours), the water content was considered as being uniform within the  
149 sample and the value of dielectric constant  $K_a$  was recorded. This operation was repeated until  
150 the specimen reached full saturation (with 1 cm water on the soil surface). All the TDR sensors

151 were calibrated in the same fashion. The results obtained on the five sensors are similar. Fig. 3  
152 presents the calibration curve of TDR for  $ITL_{10}$  along with the fitting calibration curve for  $ITL_0$   
153 presented in Duong et al. (2013) at the same dry unit mass ( $2.01 \text{ Mg/m}^3$ ). It can be observed that  
154 the curve for  $ITL_0$  lies below the curve for  $ITL_{10}$ , indicating a clear effect of soil texture. The  
155 following equation (based on the model of Topp et al. 1980) was used to fit the experimental data  
156 for  $ITL_{10}$ :

$$157 \quad [3] \quad \theta = -4.16 \times 10^{-5} \times K_a^3 + 2.11 \times 10^{-3} \times K_a^2 - 2.36 \times 10^{-2} \times K_a + 0.17$$

158         The infiltration tests were conducted in two wetting/drying cycles. After installation of the  
159 tensiometers, the saturation of soil column was completed (Saturation 1). This wetting stage was  
160 followed by a draining stage (Drainage 1). Water was allowed to drain out through the bottom  
161 valves by keeping a constant water level at the bottom of soil sample using an external water  
162 source. The first wetting/drying cycle finished by a stage of evaporation (Evaporation 1) where  
163 the top cover of the column was removed to allow soil water evaporation. A fan was used to  
164 accelerate the evaporation process. The evaporation stage ended when the suction value indicated  
165 by tensiometer T5 ( $h = 500 \text{ mm}$ ) was about 60 kPa (higher suction would lead to cavitation). A  
166 second wetting-drying cycle was applied following the same procedure (Saturation 2, Drainage 2  
167 and Evaporation 2). Before the second drainage, the hydraulic conductivity in saturated state was  
168 also measured by applying a constant water head of 0.61 m. The hydraulic gradient was 1.  
169 According to the Tennakoon et al. (2012), hydraulic gradient smaller than 4 can be considered as  
170 low enough to ensure the Darcy's law. Note that the experimental procedure with saturation from  
171 the bottom and evaporation from the top is also recommended in ASTM standard (ASTM 2010).  
172 During the measurement of hydraulic conductivity under saturated condition, the volume of water  
173 injected increased linearly with a rate of about  $50 \text{ cm}^3$  per minute.

174 The unsaturated hydraulic conductivity of *Fines* was determined using a small-scale  
 175 infiltration column of 50 mm in diameter and 200 mm in height (Munoz et al. 2008). Its  
 176 schematic view is shown in Fig. 4. Suction measurements were performed by four high-capacity  
 177 tensiometers (Cui et al. 2008) installed at 40, 80, 120 and 160 mm height from the base of the  
 178 sample. The accuracy of this tensiometer is  $\pm 1$  kPa. The soil was statically compacted in the  
 179 column in four layers of 50 mm each. Once the compaction was completed, the tensiometers  
 180 were installed. In order to ensure a good contact between the soil sample and the tensiometers, a  
 181 paste of sub-grade was applied on the surface of the ceramic of tensiometers.

182 The dry unit mass and water content of *Fines* were taken equal to those of fine particles  
 183 contained in the sample of interlayer soil. Using the illustration shown in Fig. 5, these two  
 184 parameters can be calculated as follows:

$$185 \quad [4] \quad \rho_{d,f} = \frac{M_{s,f}}{V_f} = \frac{M_s - M_{s,b}}{V - V_{s,b}} = \frac{(1-m)\rho_d V}{V - \frac{m}{\rho_{s,b}} \rho_d V} = \frac{(1-m)\rho_d \rho_{s,b}}{\rho_{s,b} - m\rho_d}$$

$$186 \quad [5] \quad w_f = \frac{M_w}{M_{s,f}} = \frac{M_s w}{M_s - M_{s,b}} = \frac{w}{1-m}$$

187 where  $M$ ,  $M_w$ ,  $M_s$  are the total mass, mass of water and mass of solid particles, respectively;  $V$ ,  $V_w$ ,  
 188  $V_s$  are the total volume, volume of water and volume of solid particles respectively;  $\rho_d$ ,  $\rho_s$  are the  
 189 dry unit mass of the specimen and unit mass of solid particles, respectively; the subscripts  $f$  and  $b$   
 190 stand for particle smaller and larger than 2 mm, respectively;  $m$  is the percentage of particles  
 191 larger than 2 mm.

192 Based on the grain size distribution curve, a value  $m = 0.67$  was determined. From Eqs (2)  
 193 and (3), a value of  $1.33 \text{ Mg/m}^3$  was obtained for the dry unit mass of *Fines*.

194           The test procedure followed for the small-scale infiltration column was akin to that for the  
195 large-scale one. After the suction stabilization, the sample was saturated from the bottom  
196 (Saturation 1). After completion of saturation, an external water source was connected to the  
197 bottom in order to ensure a constant water level after the drainage. The top cover was then  
198 removed allowing water evaporation from the soil surface (Evaporation 1). When suction at 160  
199 mm reached about 400 kPa, Evaporation 1 was stopped to avoid cavitation of the tensiometers. A  
200 second wetting-drying cycle was applied by following the same procedure as in the first cycle  
201 (Saturation 2 and Evaporation 2).

202           Unlike the large-scale column where both suction and water content were monitored, the  
203 small-scale column has only suction monitored. To obtain the water content changes during  
204 infiltration, the soil-water retention curve (SWRC) was needed. The water retention curve (WRC)  
205 of compacted *Fines* was determined separately using the device presented in Fig. 6. The soil was  
206 first compacted inside an oedometer cell (the dimensions of the soil specimen are 50 mm in  
207 diameter and 20 mm in height). The suction of the specimen was monitored by a high-capacity  
208 tensiometer fixed at the bottom of the cell. A light aluminum piston of 50 mm diameter was  
209 placed on the specimen to ensure the good contact between soil and tensiometer. The piston  
210 induced a vertical stress of 1.8 kPa and its influence was believed to be negligible. For the  
211 monitoring of soil water content, the whole system was placed on a balance having an accuracy  
212 of  $\pm 0.01$  g. The mass change indicated the quantity of water added or evaporated. More details  
213 about this cell can be found in Le et al. (2011) and Munoz-Castelblanco et al. (2012). Wetting  
214 was conducted by adding a small quantity of water on the upper face of the sample, while drying  
215 was conducted by allowing soil water evaporation from the upper surface without the piston on it.  
216 Once the desired water content was reached, the piston was put on the soil surface and the final  
217 suction was recorded. This method was also discussed by Cunningham et al. (2003); Toker et al.

218 (2004); Loucenço (2008); Loucenço et al. (2011); Toll et al. (2012) and Munoz-Castelblanco et  
219 al. (2012).

220 For the large-scale column, both suction and water content profiles were obtained  
221 directly. For the small-scale column, the suction profiles were obtained directly while the water  
222 content profiles were determined through the SWRC. The instantaneous profile method (Daniel  
223 1982; Delage and Cui 2001; Bruckler et al. 2002; Cui et al. 2008; Ye et al. 2009) was then  
224 applied for the determination of hydraulic conductivity for each soil. Note that this method is  
225 based on the generalized Darcy's law. The hydraulic gradient is determined by considering the  
226 slope of suction isochrones and the water volume passing through a given section between times  $t$   
227 and  $t+dt$  is used for calculating the water flux.

## 228 ***Experimental results***

229 The results of  $ITL_0$  were presented in Duong et al. (2013). Here only the results of  $ITL_{10}$   
230 and *Fines* are presented in detail, and the results of  $ITL_0$  are only used for comparison.

231 Fig. 7 presents changes in pore water pressure and volumetric water content versus time  
232 during Drainage 1 and Evaporation 1 for  $ITL_{10}$ . From the saturated state where the volumetric  
233 water content reached 22-25%, water drained out through the bottom valves and subsequently the  
234 volumetric water content decreased to 15 – 17% at the end of the draining stage for all the TDR  
235 sensors except that at  $h = 200$  mm (Fig. 7b). At this moment, the pore water pressure was in the  
236 range from 0 to -4 kPa (Fig. 7a). Drainage 1 finished after more than 1 day. During Evaporation  
237 1, the pore water pressure given by the tensiometer at  $h = 500$  mm decreased quickly while small  
238 changes were observed at other levels (Fig. 7a). This is consistent with the values of volumetric

239 water content: the value at  $h = 500$  m decreased significantly since the beginning of Evaporation  
240 1 while those at other levels show slight changes (Fig. 7b).

241 During Saturation 2, the external water source was set at a level applying a water pressure  
242 of 6.1 kPa to the bottom of sample. The results obtained show that less than one hour was needed  
243 to re-saturate the soil specimen (Fig. 8). The changes were not significant for T1 to T4 (small  
244 suction value), while those of T5 at  $h = 500$  mm are quite significant (Fig. 8a). Furthermore, the  
245 suction changes in Fig. 8a are consistent with those of volumetric water content in Fig. 8b. At the  
246 end of this stage when the pore water pressure became positive at all levels, the 5 tensiometers  
247 indicated the values corresponding to the water head at each level (5.5 kPa, 4.5 kPa, 3.5 kPa, 2.0  
248 kPa and 1.0 kPa for T1 to T5, respectively). The volumetric water content also reached the values  
249 of near saturated state (corresponding to the degree of saturations ranging from 87.5% to 100%).

250 The results obtained during Drainage 2 and Evaporation 2 are presented in Fig. 9. During  
251 the first two days, water inside the column was connected to the outside water source having a  
252 level decreased in steps of 50 mm from  $h = 550$  to 50 mm in order to verify the response of the  
253 sensors. Each step was kept for 1 hour. At the end of Drainage 2, the outside water source was set  
254 at  $h = 50$  mm and Evaporation 2 started. During the drainage, the volumetric water content  
255 decreased quickly while the changes of suction were much slower. As during Evaporation 1, the  
256 pore water pressure and the volumetric water content values at  $h = 500$  mm decreased  
257 significantly while the others remained almost constant. Once again, the changes of suction and  
258 volumetric water content are consistent for different levels: the closer to the evaporation surface,  
259 the higher the suction (Fig. 9a) and the smaller the volumetric water content (Fig. 9b) (except for  
260  $h = 200$  mm).

261 The inconsistent data given by the TDR sensor at  $h = 200$  mm (see Fig. 7, Fig. 8, Fig. 9)  
262 is related to the deficiency of this sensor. Indeed, some additional calibrations were conducted  
263 after the test, and the results showed some inertia of this TDR sensor: in the full range from 0 to  
264 100%, no difference with other sensors was observed; however, in a limited range, a clear  
265 difference was identified. Thereby, the results by this sensor were not considered in further  
266 analysis.

267 The data of suction and volumetric water content recorded allowed the WRC of the  
268 interlayer soil to be determined. The results are presented in Fig. 10 with three paths  
269 corresponding to Drainage 1-Evaporation 1 (Drying 1), Saturation 2 (Wetting 2) and Drainage 1-  
270 Evaporation 2 (Drying 2). It can be observed that the results of two drying processes are close. In  
271 contrast, the result of wetting path lies above. Note that because the minimum recording interval  
272 of TDR was every minute and the wetting process took place very quickly; there are less data for  
273 the wetting path. The model of van Genuchten (1980) was used to fit the experimental data with  
274 the parameters presented in Table 3.

275 The hydraulic conductivity versus suction is presented in Fig. 11, including the hydraulic  
276 conductivity measured at saturated state, equal to  $1.67 \times 10^{-5}$  m/s. It can be seen that the results for  
277 the two drying paths are similar, suggesting negligible microstructure changes. For the wetting  
278 path, all results lie above those of the drying paths, illustrating a clear phenomenon of hysteresis.  
279 The models of van Genuchten (1980) and Brooks-Corey (Brooks and Corey 1964; Stankovich  
280 and Lockington 1995) were used for fitting the data of both drying and wetting paths using the  
281 least squares method (see Fig. 11). The parameters determined are presented in Table 4 .

282 Fig. 12 presents the comparison between the WRC of  $ITL_0$  and  $ITL_{10}$  for the drying path  
283 (the parameters of van Genuchten's model (1980) used for fitting the experimental data are

284 presented in Table 3). Note that for clarity, the scattered data at low suction are not included. The  
285 WRC of  $ITL_0$  is beneath the WRC of  $ITL_{10}$ , suggesting that at a given suction,  $ITL_{10}$  has a higher  
286 water content than  $ITL_0$ . This appears normal because with the same dry unit mass, the higher the  
287 fines content, the higher the retention capacity.

288 The comparison of hydraulic conductivity between  $ITL_0$  and  $ITL_{10}$  is presented in Fig. 13.  
289 In the saturated state, the two soils have almost the same value:  $1.67 \times 10^{-5}$  m/s for  $ITL_{10}$  and  
290  $1.75 \times 10^{-5}$  m/s for  $ITL_0$ . Both values are lower than the critical value proposed by Selig and  
291 Waters (1994) for the railway substructures. In unsaturated state, even the data are scattered for  
292 the two soils, an identical trend can be identified: the hydraulic conductivity is decreasing with  
293 the increase of suction. Moreover, the average value for  $ITL_{10}$  is slightly higher than that for  $ITL_0$ ,  
294 suggesting a slightly greater hydraulic conductivity for  $ITL_{10}$ . On the whole, the difference  
295 between the hydraulic conductivity results of two soils is less evident than the difference between  
296 the SWRC results.

297 The results obtained from the small-scale infiltration test on *Fines* are shown in Fig. 14 to  
298 Fig. 18. After installation of the tensiometers, a period of 18 hours was needed to reach the  
299 suction equilibrium at 70 – 83 kPa (Fig. 14). This difference in final suctions at different levels  
300 was mainly related to the soil heterogeneity. The corresponding degree of saturation was 43%.  
301 From this initial state, the soil was first re-saturated by injecting water from the bottom with a  
302 constant water head of 0.7 kPa. The suction at the lowest level changed first, followed by the  
303 suctions at higher levels (Fig. 15). Ten minutes after the water injection, water appeared on the  
304 upper surface and suctions at all level reached zero, indicating the full saturation of the soil  
305 specimen.

306           After Saturation 1, water was drained out to an outside water source and the water level  
307 was maintained at  $h = 0$ . Afterwards, Evaporation 1 took place. The results obtained are shown in  
308 Fig. 16. Fifteen hours later, the pore water pressure measured at  $h = 160$  mm (40 mm below the  
309 soil surface) started to decrease and reached -300 kPa at 57 hours. The changes in water pressures  
310 measured by other tensiometers were less significant.

311           Saturation 2 took place right after Evaporation 1. The results obtained during this second  
312 wetting stage are shown in Fig. 17. Less than 2 minutes was required for the pore water pressure  
313 at  $h = 160$  mm to come back from -300 kPa to about 0. The results obtained during the  
314 subsequent drying are shown in Fig. 18 (Evaporation 2). As in the case of Evaporation 1, after 80  
315 hours, the pore water pressure at  $h = 160$  mm decreased to - 365 kPa while those at other levels  
316 did not change significantly.

317           The results from the test in the tensiometer-equipped oedometer are shown in Fig. 19. Fig.  
318 19a depicts the suction (negative pore water pressure given by the tensiometer) evolution after the  
319 tensiometer installation. The suction increased and reached its stabilization value of 110 kPa after  
320 17 hours. This corresponds to the initial state of the soil specimen (21.3 % volumetric water  
321 content and 42.6 % degree of saturation). Water was then added into the specimen to follow the  
322 wetting path. The variation of the first step of wetting is presented in Fig. 19b. About 35 minutes  
323 was needed for suction stabilization. The volumetric water content in this step increased from  
324 21.3% to 21.7%. This operation was repeated until the soil reached the near saturated state. Then  
325 the drying steps started. Fig. 19c presents the suction stabilization during one drying step. An  
326 equilibrium value of 79 kPa was reached after 320 minutes. This suction increase corresponded to  
327 a decrease of volumetric water content from 22.2% to 21.6%.

328           The SWRC obtained for *Fines* is shown in Fig. 20. From its initial state, the soil specimen  
329 was subjected to wetting up to 70% degree of saturation, followed by drying and finally a second  
330 wetting till full saturation. It can be seen that the SWRC obtained during drying lies above that  
331 during wetting. The maximum suction value was 390 kPa corresponding to a volumetric water  
332 content of 18.9%; it was also close to the maximum suction value in the specimen during the  
333 infiltration test, indicating the compatibility of the two tests.

334           This SWRC determined was then used to calculate the changes of volumetric water  
335 content in the small-scale infiltration column based on the suction changes presented in Fig. 15 to  
336 Fig. 18. Either the drying or the wetting path was used depending on the path followed in the  
337 infiltration test. As the second drying path of SWRC was not available, the first drying path was  
338 used for calculating the volumetric water content during the second drying path in the infiltration  
339 test. Then, based on the profiles of suction and water content, the hydraulic conductivity of  
340 compacted *Fines* was calculated. The results are shown in Fig. 21, including the hydraulic  
341 conductivity measured at saturated state by applying a constant water pressure of 0.7 kPa:  
342  $2.6 \times 10^{-6}$  m/s. Albeit the large data scatter, a clear trend can be observed: as for the interlayer soil,  
343 the hydraulic conductivity increased when the suction decreased.

344           It is worth noting that the results obtained for the two drying paths are quite similar. The  
345 same conclusion can be drawn for the two wetting paths. The models of van Genuchten (1980)  
346 and Brooks-Corey (Brooks and Corey 1964; Stankovich and Lockington 1995) were used to fit  
347 the results (Fig. 21), and the parameters determined are presented in Table 4. Comparison  
348 between the drying and wetting curves shows that for the 2 wetting/drying cycles, the wetting  
349 curves lie always above the drying curves. It is opposed to the SWRC where the wetting curves  
350 are normally beneath the drying ones. In addition, the curves of wetting path and drying path of

351 the 1<sup>st</sup> cycle are close to those corresponding to the 2<sup>nd</sup> cycle, suggesting no effect of  
352 wetting/drying cycles on the hydraulic conductivity. The smallest value of hydraulic conductivity  
353 identified is  $6 \times 10^{-12}$  m/s corresponding to a suction value of 242 kPa, while the highest one is  
354  $2.6 \times 10^{-6}$  m/s corresponding to the saturated state.

355 Fig. 22 depicts the comparison of SWRC between *ITL<sub>10</sub>* and *Fines* in the plane of degree  
356 of saturation versus suction. The two curves start from almost the same point - around 97%  
357 degree of saturation and 1.7 kPa suction. From 3 kPa suction, the WRC of *ITL<sub>10</sub>* starts to separate  
358 from the WRC of *ITL<sub>0</sub>*. The two curves are parallel (for drying path) from 10 kPa suction. The  
359 curves of *ITL<sub>10</sub>* stop at 71 kPa while the curves of *Fines* stop at 389 kPa due to the different  
360 capacities of the tensiometers used for the two soils. The gap between two curves is about 10% of  
361 degree of saturation at the end of the curve for *ITL<sub>10</sub>*.

362 In Fig. 23, the hydraulic conductivity of *ITL<sub>10</sub>* and *Fines* is plotted versus suction. It can  
363 be observed that the wetting and drying curves of the interlayer soil are quite close to those of  
364 *Fines*, suggesting that the hydraulic conductivity of the interlayer soil is mainly governed by the  
365 hydraulic conductivity of the fines contained in it. In other words, water transfer in the interlayer  
366 soil takes place mainly through the network of pores between fine particles, coarse elements like  
367 ballast behaving as inert materials. This is confirmed by the hydraulic conductivity values at  
368 saturated state: similar values were identified -  $1.67 \times 10^{-5}$  m/s for *ITL<sub>10</sub>* against  $2.6 \times 10^{-6}$  m/s for  
369 *Fines*.

370 From a practical point of view, Fig. 23 shows that to determine the hydraulic conductivity  
371 of interlayer soils, it is not necessary to use large-scale experimental devices to match the soil  
372 grain size; smaller devices can be used to determine their hydraulic conductivity by testing the  
373 fine particles only, provided that equivalent dry density is accounted for.

374 **Discussions**

375 Fig. 11 and Fig. 21 show the uncommon phenomenon of hysteresis observed in hydraulic  
376 conductivity of *ITL<sub>10</sub>* and *Fines*, respectively. The curve of wetting path lies above the curve of  
377 drying path. The same phenomenon was observed by Wayllace and Lu (2011). The following  
378 interpretations can be attempted.

379         Due to the different kinetic between the fast liquid transfer in wetting and the long vapor  
380 transfer in drying, the time needed for drying was much longer than that for wetting. This  
381 phenomenon was also reported by Toker et al. (2004) and discussed by Munoz-Castelblanco et  
382 al. (2012). A higher hydraulic conductivity can be expected in that case for wetting path.

383         In the present work, the calculation of hydraulic conductivity was performed based on the  
384 suction evolution given by tensiometers. Assuming that in the compacted soils, both macro-pores  
385 and micro-pores existed. During wetting, the macro-pores were filled with water more quickly  
386 than micro-pores. Moreover, in the micro-pores, there were always air bubbles preventing the  
387 total saturation. In contrast, during drying, all pores (micro and macro) participated in the  
388 evaporation process. As a result, when water filled the macro-pores, the tensiometers  
389 immediately gave the suction changes corresponding to the water flow through the macro-pores,  
390 even though the suction in micro-pores would be higher. On the contrary, when water evaporates  
391 during drying, the tensiometers gave the suction changes that involve both macro and micro-  
392 pores, in a much slower fashion. In other words, the suction measured by the tensiometers was  
393 probably under-estimated for wetting paths. Côté and Roy (1998) also reported that one re-  
394 saturating stage is not enough to fully saturate a soil sample because of the air bubbles trapped in  
395 micro-pores. This can also explain the uncommon hysteresis mentioned before.

396 Poulouvassilis (1969) (cited by Mualem 1976) considered, in a qualitative way, the  
397 influence of capillary hysteresis on the hydraulic conductivity based on the concept of  
398 independent domain theory. He defined two mechanisms related to hysteresis: (i) water fills pores  
399 of larger opening radius in a wetting process than in drying one; (ii) the pores configuration and  
400 interconnection may be different for wetting and drying. As a result, the hydraulic conductivity in  
401 wetting may be different from that in drying for the same water content. The theory about the  
402 difference between the opening radius affecting wetting process and the opening radius affecting  
403 drying process is known as the effect of ink-bottle (Bertotti and Mayergoyz 2006; Naumov  
404 2009). According to this theory, the pores affecting the wetting curve are larger than the pores  
405 affecting the drying curve. As a result, the water transfer is faster during wetting than during  
406 drying, implying a higher hydraulic conductivity in the case of wetting.

## 407 **Conclusions**

408 Infiltration tests were performed on the interlayer soil ( $ITL_0$ ) and its derived soils - adding 10% of  
409 sub-grade to form  $ITL_{10}$  and sieving  $ITL_{10}$  at 2 mm to form *Fines*. Two wetting/drying cycles  
410 were applied for each test. The obtained results allowed the effect of fine particles on the water  
411 retention capacity and hydraulic conductivity of interlayer soil to be analyzed.

412 The effect of wetting/drying cycles on hydraulic conductivity was found negligible - the  
413 results of the first cycle are quite similar to those of the second cycle, suggesting an insignificant  
414 microstructure change by wetting/drying cycles.

415 Hysteresis exists for both the soil water retention curve and the hydraulic conductivity  
416 changes with suction. The wetting process was found to be much faster than the drying process,  
417 and the hydraulic conductivity during wetting is always higher than that during drying. This can

418 be explained by the effect of ink-bottle and the difference between the water transfer through the  
419 network of macro-pores and micro-pores.

420 Adding 10% fine particles to the natural interlayer soil changes the soil water retention  
421 curve but does not induce significant changes in hydraulic conductivity. In saturated state, the  
422 hydraulic conductivity of natural interlayer soil is  $1.75 \times 10^{-5}$  m/s, while the value of the soil with  
423 10% fines added is  $1.67 \times 10^{-6}$  m/s. In unsaturated state, even though the results are little scattered,  
424 the results of  $ITL_{10}$  are within the variation range of the results of  $ITL_0$ . However, it is worth  
425 noting that the mean value of  $ITL_{10}$  is slightly greater than that of  $ITL_0$ .

426 The water retention curves of  $ITL_{10}$  and *Fines* are different, illustrating an obvious effect  
427 of soil texture. On the contrary, in terms of hydraulic conductivity including the values in  
428 saturated state, a good agreement was identified between the results of two soils, regardless of the  
429 drying or wetting paths. This suggests that water transfer in the interlayer soil takes place mainly  
430 through the network of pores between fine particles, coarse elements like ballast behaving as inert  
431 materials. From a practical point of view, this finding shows that to determine the hydraulic  
432 conductivity of interlayer soils, a device as small as the small-scale infiltration cell can be  
433 employed to determine the hydraulic conductivity of interlayer soil by testing the fine particles  
434 only, provided that equivalent dry density is taken into account.

435

## 436 ***Acknowledgements***

437 The present work is part of the project RUFEX (Re-use of ancient railway platforms and existing  
438 foundations) funded by the French National Research Agency. The supports of French Railway  
439 Company (SNCF) and Ecole des Ponts ParisTech are also gratefully acknowledged.

440 **Reference**

- 441 Alobaidi, I., and Hoare, D. 1996. The development of pore water pressure at the sub-grade-  
442 subbase interface of a highway pavement and its effect on pumping of fines. *Geotextiles and*  
443 *geomembranes*, **14**: 111-135.
- 444 Alobaidi, I., and Hoare, D. 1998. The role of geotextile reinforcement in the control of pumping  
445 at the sub-grade-subbase interface of highway pavements. *Geosynthetics International*, **5**(6): 619–  
446 636.
- 447 AFNOR. 2005. Identification and classification of soil- Part 2: Principles for a classification. NF  
448 EN ISO 14688.
- 449 Anbazhagan, P., Lijun, S., Buddhima, I., and Cholachat, R. 2011. Model track studies on fouled  
450 ballast using ground penetrating radar and multichannel analysis of surface wave. *Journal of*  
451 *Applied Geophysics*, **74**(4): 175–184.
- 452 ASTM 2010. Standard test method for measurement of hydraulic conductivity of unsaturated  
453 soils. D7664-10.
- 454 Ayres, D. 1986. Geotextiles or geomembranes in track? British railways' experience. *Geotextiles*  
455 *and Geomembranes*, **3**(2-3): 129–142.
- 456 Babic, B., Prager, A., and Rukavina, T. 2000. Effect of fine particles on some characteristics of  
457 granular base courses. *Materials and Structures*, **7**(33): 419-424.
- 458 Bertotti, G., and Mayergoyz, I. D. 2006. *The science of hysteresis III*. Academic Press
- 459 Brooks, R.H., and Corey, A.T., 1964. Hydraulic properties of porous media. Hydro. Paper No.3,  
460 Colorado State Univ., Fort Collins, Colo.
- 461 Bruckler, L. B., Angulo-Jaramillo, P., and Ruy, R. 2002. Testing an infiltration method for  
462 estimating soil hydraulic properties in the laboratory. *Soil Science Society of America Journal*,  
463 **66**: 384–395.
- 464 Cabalar, A. 2008. Effect of fines content on the behavior of mixed specimens of a sand.  
465 *Electronic Journal of Geotechnical Engineering*, **13**(D): 1-11.
- 466 Côté, J., and Roy, M. 1998. Conductivité hydraulique de matériaux de fondations de chaussées  
467 partiellement saturés (In French). *Rapport de l'études et recherches en transports du Québec*,  
468 177p.
- 469 Cui, Y.J., Duong, T.V., Tang, A.M., Dupla, J.C., Calon, N., and Robinet, A. 2013. Investigation  
470 of the hydro-mechanical behaviour of fouled ballast. *Journal of Zhejiang University-Science A*  
471 *(Applied Physics & Engineering)*, **14**(4): 244-255.

- 472 Cui, Y. J., Tang, A. M., Mantho, A., and Delaure, E. 2008. Monitoring field soil suction using a  
473 miniature tensiometer. *Geotechnical Testing Journal*, **31**(1) : 95-100.
- 474 Cui, Y. J., Tang, A. M., Loiseau, C., and Delage, P. 2008. Determining the unsaturated hydraulic  
475 conductivity of a compacted sand-bentonite mixture under constant-volume and free-swell  
476 conditions. *Physics and Chemistry of the Earth, Parts A/B/C*, **33**: S462–S471.
- 477 Cunningham, M., Ridley, A., Dineen, K., and Burland, J. 2003. The mechanical behaviour of a  
478 reconstituted unsaturated silty clay. *Géotechnique*, **53** (2): 183-194.
- 479 Daniel, D. E. 1982. Measurement of hydraulic conductivity of unsaturated soils with  
480 thermocouple psychrometers. *Soil Science Society of American Journal*, **46**(6): 1125–1129.
- 481 Delage, P., and Cui, Y. J. 2001. Comportement mécanique des sols non saturés. Article C302. Ed.  
482 *Techniques Ingénieur*.
- 483 Duong, T. V., Tang, A. M., Cui., Y. J., Trinh, V. N., and Calon, N. 2013. Development of a  
484 large-scale infiltration column for studying the hydraulic conductivity of unsaturated fouled  
485 ballast. *Geotechnical Testing Journal*, **36**(1): 55-63.
- 486 Ebrahimi, A. 2011. Behavior of fouled ballast. *Railway Track and Structures*, **107**(8): 25–31.
- 487 Fortunato, E., Pinelo, A., and Matos Fernandes, M. 2010. Characterization of the fouled ballast  
488 layer in the substructure of a 19th century railway track under renewal. *Soils and Foundations*,  
489 **50**(1): 55–62.
- 490 Ghataora, G., Burns, B., Burrow, M., and Evdorides, H. 2006. Development of an index test for  
491 assessing anti-pumping materials in railway track foundations. *Proc., First International*  
492 *Conference on Railway Foundations*. 355–366.
- 493 Giannakos, K. 2010. Loads on track, ballast fouling, and life cycle under dynamic loading in  
494 railways. *Journal of Transportation Engineering*, **136**(12): 1075–1084.
- 495 Gong, Y., Cao, Q., and Sun, Z. 2003. The effects of soil bulk density, clay content and  
496 temperature on soil water content measurement using time-domain reflectometry. *Hydrological*  
497 *Processes*, **17**(18): 3601–3614.
- 498 Huang, H., Tutumluer, E., and Dombrow, W. 2009. Laboratory characterization of fouled  
499 railroad ballast behavior. *Transportation Research Record: Journal of the Transportation*  
500 *Research Board*, **2117**(1): 93–101.
- 501 Indraratna, B., Salim, W., and Rujikiatkamjorn, C. 2011. *Advanced Rail Geotechnology -*  
502 *Ballasted Track*. CRC Press.
- 503 Jacobsen, O. H., and Schjønning, P. 1993. A laboratory calibration of time domain reflectometry  
504 for soil water measurement including effects of bulk density and texture. *Journal of Hydrology*,  
505 **151**(2-4): 147–157.

- 506 Kim, D., Sagong, M., and Lee, Y. 2005. Effects of fine aggregate content on the mechanical  
507 properties of the compacted decomposed granitic soils. *Construction and Building Materials*,  
508 **19**(3): 189–196.
- 509 Le, T.T., Cui, Y.J., Muñoz, J.J., Delage, P., Tang, A.M., and Li; X.L. 2011. Studying the stress-  
510 suction coupling in soils using an oedometer equipped with a high capacity tensiometer. *Frontiers*  
511 *of Architecture and Civil Engineering in China* **5**(2): 160-170.
- 512 Lourenço, S. 2008. Suction measurements and water retention in unsaturated soils.  
513 PhD dissertation, Durham University.
- 514 Lourenço, S., Gallipoli, D., Toll, D., Augarde, C., and Evans, F. 2011. A new procedure for the  
515 determination of soil-water retention curves by continuous drying using high-suction  
516 tensiometers. *Canadian Geotechnical Journal*, **48**(2): 327-335
- 517 Mayoraz, F., Vulliet, L., and Laloui, L. 2006. Attrition and particle breakage under monotonic  
518 and cyclic loading. *Comptes Rendus Mécanique*, **334**(1): 1–7.
- 519 Mualem, Y. 1976. Hysteretical models for prediction of the hydraulic conductivity of unsaturated  
520 porous media. *Water Resources Research*, **12**(6): 1248-1254.
- 521 Munoz, J. J., De Gennaro, V., and Delaure, E. 2008. Experimental determination of unsaturated  
522 hydraulic conductivity in compacted silt. In *Unsaturated soils: advances in geo-engineering:*  
523 *proceedings of the 1st European Conference on Unsaturated Soils, E-UNSAT 2008, Durham,*  
524 *United Kingdom, 2-4 July 2008, pp.123-127.*
- 525 Munoz-Castelblanco, J. A., Pereira, J. M., Delage, P., and Cui, Y. J. 2012. The water retention  
526 properties of a natural unsaturated loess from northern France. *Géotechnique*, **62**(2): 95-106.
- 527 Naumov, S. 2009. Hysteresis phenomenon in Mesoporous Materials. PhD Dissertation,  
528 University of Leipzig.
- 529 Naeini, S., and Baziar, M. 2004. Effect of fines content on steady-state strength of mixed and  
530 layered specimens of a sand. *Soil Dynamics and Earthquake Engineering*, **24**(3): 181–187.
- 531 Pedro, L. 2004. De l'étude du comportement mécanique de sols hétérogènes modèles à son  
532 application au cas des sols naturels. PhD disertation, Ecole Nationale des Ponts et Chaussées,  
533 France. (In French).
- 534 Poulouvassilis, A. 1969. The effect of hysteresis of pore water on the hydraulic conductivity. *Soil*  
535 *Science*, **20**: 52-56.
- 536 Schneider, J. M., and Fratta, D. 2009. Time-domain reflectometry - parametric study for the  
537 evaluation of physical properties in soils. *Canadian Geotechnical Journal*, **46**(7): 753–767.
- 538 Selig, E. T., and Waters, J. M. 1994. *Track geotechnology and substructure management.*  
539 *Thomas Telford.*

- 540 Seif El Dine, S., Dupla, J., Frank, R., Canou, J., and Kazan, Y. 2010. Mechanical characterization  
541 of matrix coarse-grained soils with a large-sized triaxial device. *Canadian Geotechnical Journal*,  
542 **47**(4): 425–438.
- 543 Stankovich J. M., and Lockington, D. A., 1995. Brooks-Corey and van Genuchten, soil-water-  
544 retention models. *Journal of Irrigation and Drainage Engineering*, 121(1): 1-7.
- 545 Stolte, J., Veerman, M., Wosten, G. J., Freijer, J. H. M., Bouten, J. I., Dirksen, W., Van Dam,  
546 C., and Van den Berg, J.C. 1994. Comparison of six methods to determine unsaturated soil  
547 hydraulic conductivity. *Soil Science Society of America Journal*, **58**(6): 1596-1603.
- 548 Sussmann, T. R., Ruel, M., and Christmer, S. 2012. Sources, influence, and criteria for ballast  
549 fouling condition assessment. Proc., 91st Annual Meeting of the Transportation Research Board.  
550 11p.
- 551 Tennakoon, N., Indraratna, B., Rujikiatkamjorn, C., Nimbalkar, S., and Neville, T. 2012. The role  
552 of ballast-fouling characteristics on the drainage capacity of a rail substructure. *Geotechnical*  
553 *Testing Journal*, **35**(4): 1-12.
- 554 Toker, N., Germaine, J., Sjoblomt, K. and Culligan, P. 2004. A new technique for rapid  
555 measurement of continuous soil moisture characteristic curves. *Géotechnique*, **54**(3): 179-186.
- 556 Toll, D., Lourenço, S., and Mendes, J. 2012. Advances in suction measurements using high  
557 suction tensiometers. *Engineering Geology*. doi.org/10.1016/j.enggeo.2012.04.013.
- 558 Topp, G. C., Davis, J. L., and Annan, A. P. 1980. Electromagnetic determination of soil water  
559 content: measurements in coaxial transmission lines. *Water Resource Research*, (16): 574-582.
- 560 Trinh, V.N. 2011. Comportement hydromécanique des matériaux constitutifs de plateformes  
561 ferroviaires anciennes. (In French). PhD Dissertation, Ecole Nationales des Ponts et Chaussées -  
562 Université Paris – Est.
- 563 Trinh, V. N., Tang, A. M., Cui, Y. J., Canou, J., Dupla, J.C., Calon, N., Lambert, L., Robinet,  
564 A., and Schoen, O. 2011. Caractérisation des matériaux constitutifs de plate-forme ferroviaire  
565 ancienne. (In French). *Revue Française de Géotechnique*, (134-135): 65–74.
- 566 Trinh, V.N., Tang, A.M., Cui, Y.J., Dupla, J.C., Canou, J., Calon, N., Lambert, L., Robinet, A.,  
567 and Schoen, O. 2012. Mechanical characterisation of the fouled ballast in ancient railway track  
568 substructure by large-scale triaxial tests. *Soils and Foundations*, **52**(3): 511-523.
- 569 van Genuchten, M.T. 1980. A closed-form equation for predicting the hydraulic conductivity of  
570 unsaturated soils. *Soil Science Society of America Journal*, **44**(5): 892–898.
- 571 Verdugo, R., and Hoz, K. 2007. Strength and stiffness of coarse granular soils. *Solid Mechanics*  
572 *and Its Application*, **146**(3): 243–252.

573 Wayllace, A., and Lu, N. 2011. A transient water release and imbibitions method for rapidly  
574 measuring wetting and drying soil water retention and hydraulic conductivity functions.  
575 Geotechnical Testing Journal, **35**(1): 1-15.

576 Ye, W. M., Cui, Y. J., Qian, L. X., and Chen, B. 2009. An experimental study of the water  
577 transfer through compacted GMZ bentonite. Engineering Geology, **108**(3): 169– 176.

578

579 **List of table**

- 580 Table 1: Properties of the soil studied  
581 Table 2: Fouling state of the interlayer soil  
582 Table 3: Parameters of the van Genuchten's model (1980) for the soil water retention curves of  
583 interlayer soil  
584 Table 4: Parameters of the van Genuchten's model and Brooks-Corey's model for the hydraulic  
585 conductivity of  $ITL_{10}$  and *Fines*

586

587 **List of figures**

- 588 Fig. 1: Grain size distribution curves of the interlayer soil ( $ITL_0$ ) and its derived ones ( $ITL_{10}$  and  
589 *Fines*)  
590 Fig. 2: Schematic view of the large-scale infiltration column  
591 Fig. 3: Calibration curves of the TDRs used for the  $ITL_{10}$  and  $ITL_0$  specimens  
592 Fig. 4: Schematic view of the small-scale infiltration column  
593 Fig. 5: Components of the unsaturated interlayer soil  
594 Fig. 6: Device for determining the WRC of *Fines*  
595 Fig. 7: Test on  $ITL_{10}$ : pore water pressure and volumetric water content evolutions during  
596 Drainage 1 and Evaporation 1  
597 Fig. 8: Test on  $ITL_{10}$ : pore water pressure and volumetric water content evolutions in Saturation 2  
598 Fig. 9: Test on  $ITL_{10}$ : pore water pressure and volumetric water content evolutions during  
599 Drainage 2 and Evaporation 2  
600 Fig. 10: WRC of  $ITL_{10}$  with fitting curves using the van Genuchten's model (1980)  
601 Fig. 11: Hydraulic conductivity of  $ITL_{10}$  obtained with drying-wetting cycles  
602 Fig. 12: Comparison of SWRC between  $ITL_0$  and  $ITL_{10}$   
603 Fig. 13: Comparison of hydraulic conductivity between  $ITL_0$  and  $ITL_{10}$   
604 Fig. 14: Test on *Fines*: suction stabilization after the installation of tensiometers  
605 Fig. 15: Test on *Fines*: suction evolutions during Saturation 1  
606 Fig. 16: Test on *Fines*: suction evolutions during Evaporation 1  
607 Fig. 17: Test on *Fines*: suction evolutions during Saturation 2  
608 Fig. 18: Test on *Fines*: suction evolutions during Evaporation 2  
609 Fig. 19: Stabilization of suction during the SWRC determination. (a) initial stabilization after  
610 tensiometer installation, (b) a wetting stage, (c) a drying stage  
611 Fig. 20: WRC of *Fines*  
612 Fig. 21: Hydraulic conductivity of *Fines*, obtained with drying/wetting cycles  
613 Fig. 22: Comparison of SWRC between  $ITL_{10}$  and *Fines*  
614 Fig. 23: Comparison of hydraulic conductivity between  $ITL_{10}$  and *Fines*

615

616 **Table 1: Properties of the soil studied**

| Soil                                    | Properties                                               | Value                  |
|-----------------------------------------|----------------------------------------------------------|------------------------|
| Interlayer soil ( $ITL_0$ )             | $\rho_s$ (particles smaller than 2 mm)                   | 2.67 Mg/m <sup>3</sup> |
|                                         | $\rho_s$ (particles larger than 2 mm)                    | 2.68 Mg/m <sup>3</sup> |
|                                         | $d_{10}$                                                 | 0.01 mm                |
|                                         | $d_{30}$                                                 | 5 mm                   |
|                                         | $d_{60}$                                                 | 30 mm                  |
|                                         | liquid limit $w_L$ (smaller than 100 $\mu\text{m}$ )     | 40.2%                  |
|                                         | plasticity index $I_p$ (smaller than 100 $\mu\text{m}$ ) | 11.3%                  |
| Sub-grade (Fines to create $ITL_{10}$ ) | liquid limit $w_L$                                       | 57.8%                  |
|                                         | plasticity index $I_p$                                   | 24.1%                  |

617

618

619 **Table 2: Fouling state of the interlayer soil**

|            | Fouling Index | Relative ballast fouling ratio | Fouling category |
|------------|---------------|--------------------------------|------------------|
|            | $FI$ (-)      | $R_{b-f}$ (%)                  |                  |
| $ITL_0$    | 45            | 56                             | Highly fouled    |
| $ITL_{10}$ | 59            | 72                             | Highly fouled    |

620

621 **Table 3: Parameters of the van Genuchten's model (1980) for the soil water retention curves of interlayer soil**

|                                                                                   | Natural interlayer soil<br>( <i>ITL<sub>0</sub></i> ) | Interlayer soil with 10% sub-soil added ( <i>ITL<sub>10</sub></i> ) |                   |                   |
|-----------------------------------------------------------------------------------|-------------------------------------------------------|---------------------------------------------------------------------|-------------------|-------------------|
| Formula                                                                           | Drying                                                | Drying 1                                                            | Wetting 2         | Drying 2          |
| $\theta = \theta_r + \frac{\theta_s - \theta_r}{\left[1 + (\alpha h)^n\right]^m}$ | $\theta_s = 25$                                       | $\theta_s = 25$                                                     | $\theta_s = 22.5$ | $\theta_s = 25$   |
|                                                                                   | $\theta_r = 0$                                        | $\theta_r = 10$                                                     | $\theta_r = 10$   | $\theta_r = 10$   |
|                                                                                   | $\alpha = 4$                                          | $\alpha = 159.62$                                                   | $\alpha = 0.19$   | $\alpha = 113.45$ |
|                                                                                   | $n = 1.17$                                            | $n = 1.24$                                                          | $n = 5.24$        | $n = 1.25$        |
|                                                                                   | $m = 0.15$                                            | $m = 0.19$                                                          | $m = 0.81$        | $m = 0.2$         |

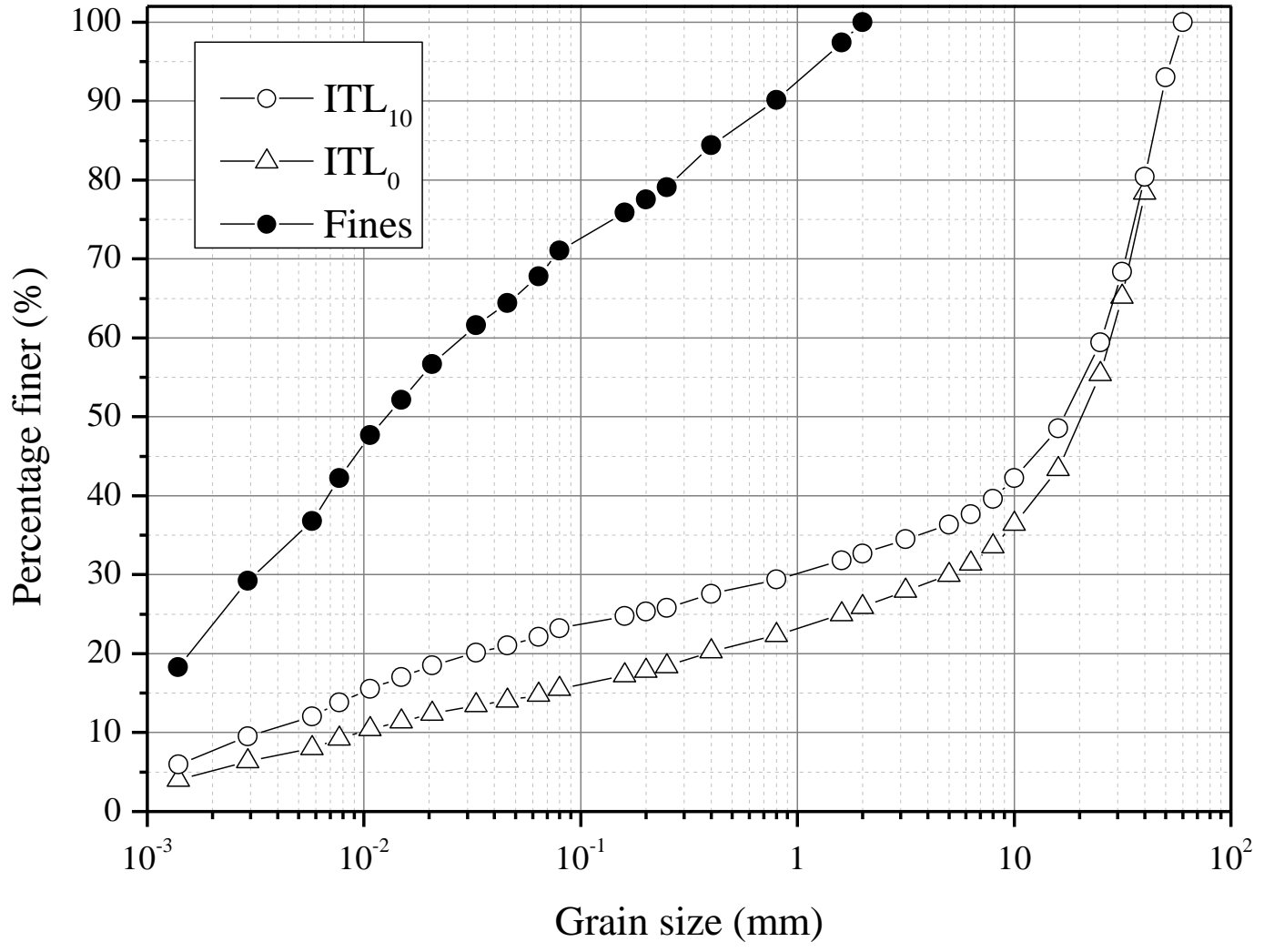
622 *Notes:*  $\theta$  is volumetric water content (%);  $\theta_s$  is the volumetric water content at saturated state (%);  
 623  $\theta_r$  is the residual volumetric water content (%);  $h$  is hydraulic head in meter;  $\alpha$ ,  $n$ ,  $m$  are the  
 624 model's parameters

625 **Table 4: Parameters of the van Genuchten's model and Brooks-Corey's model for the hydraulic conductivity**  
 626 **of *ITL<sub>10</sub>* and *Fines***

| Model         | Formula                                                                                                      | Soil                    | Drying path                                         | Wetting path                                      |
|---------------|--------------------------------------------------------------------------------------------------------------|-------------------------|-----------------------------------------------------|---------------------------------------------------|
| van Genuchten | $k = k_s \frac{1 - (\alpha h)^{n-2} \left[1 + (\alpha h)^n\right]^{-m}}{\left[1 + (\alpha h)^n\right]^{2m}}$ | <i>ITL<sub>10</sub></i> | $\alpha = 7.16$<br><br>$n = 2.12$<br><br>$m = 0.06$ | $\alpha = 0.5$<br><br>$n = 2.4$<br><br>$m = 0.17$ |
|               |                                                                                                              | <i>Fines</i>            | $\alpha = 2.1$<br><br>$n = 2.06$                    | $\alpha = 0.25$<br><br>$n = 2.37$                 |

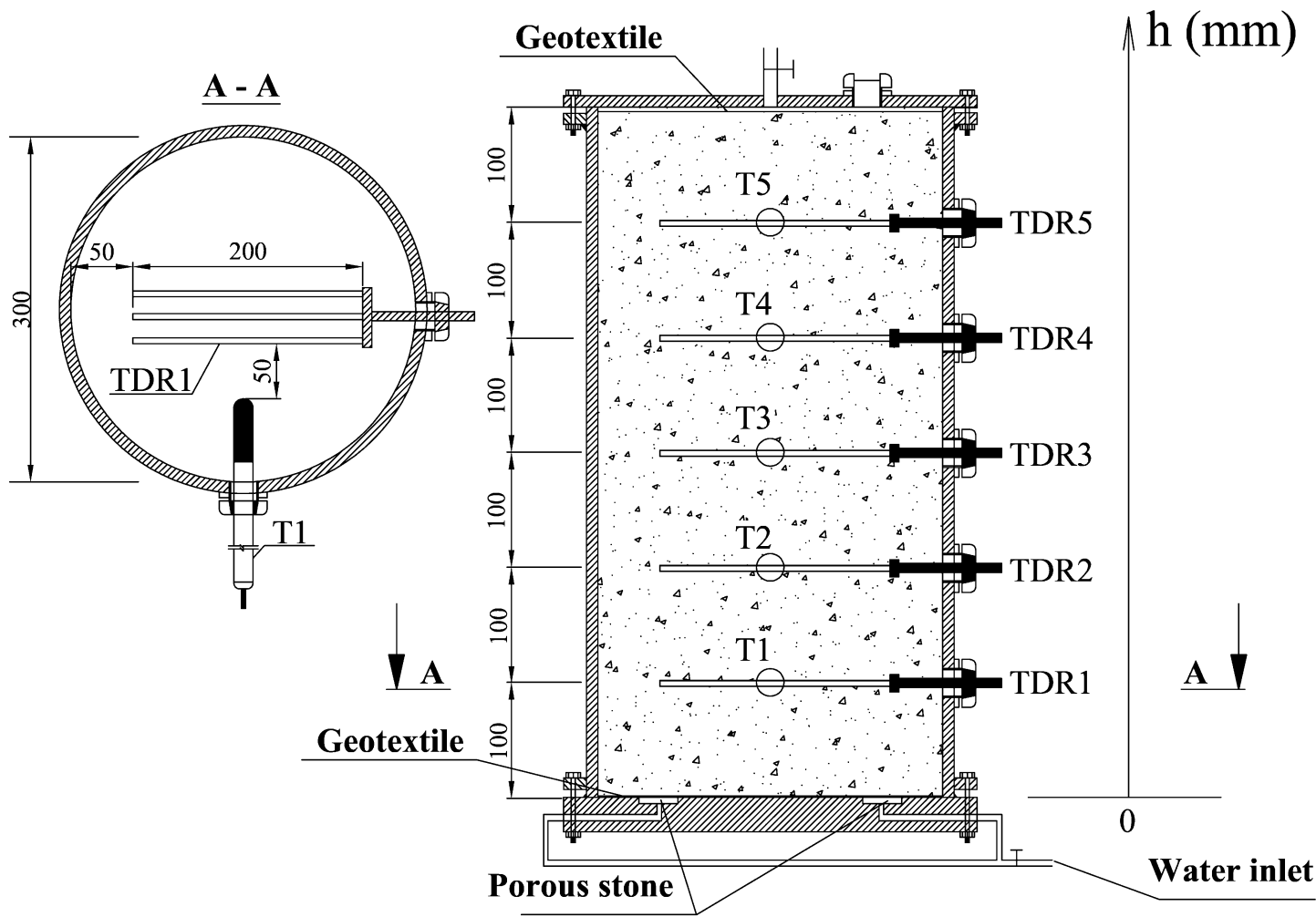
|              |                                                     |                         |                                           |                                           |
|--------------|-----------------------------------------------------|-------------------------|-------------------------------------------|-------------------------------------------|
|              |                                                     |                         | $m = 0.03$                                | $m = 0.15$                                |
|              |                                                     | For the two soils       | $\alpha = 2.2$<br>$n = 2.1$<br>$m = 0.05$ | $\alpha = 0.3$<br>$n = 2.7$<br>$m = 0.16$ |
| Brooks-Corey | $k = k_s \left( \frac{s_a}{s} \right)^{2+3\lambda}$ | <i>ITL<sub>10</sub></i> | $s_a = 0.3$<br>$\lambda = 0.05$           | $s_a = 4$<br>$\lambda = 0.1$              |
|              |                                                     | <i>Fines</i>            | $s_a = 0.7$<br>$\lambda = 0.01$           | $s_a = 7$<br>$\lambda = 0.01$             |
|              |                                                     | For the two soils       | $s_a = 0.74$<br>$\lambda = 0.03$          | $s_a = 5.4$<br>$\lambda = 0.02$           |

627 Notes:  $k$  is the hydraulic conductivity;  $k_s$  is the hydraulic conductivity in saturated state;  $h$  is  
628 hydraulic head in meter;  $s$  is the suction (kPa);  $s_a$  is the air-entry value (kPa);  $\lambda$ ,  $\alpha$ ,  $n$ ,  $m$  are  
629 parameters of the models.



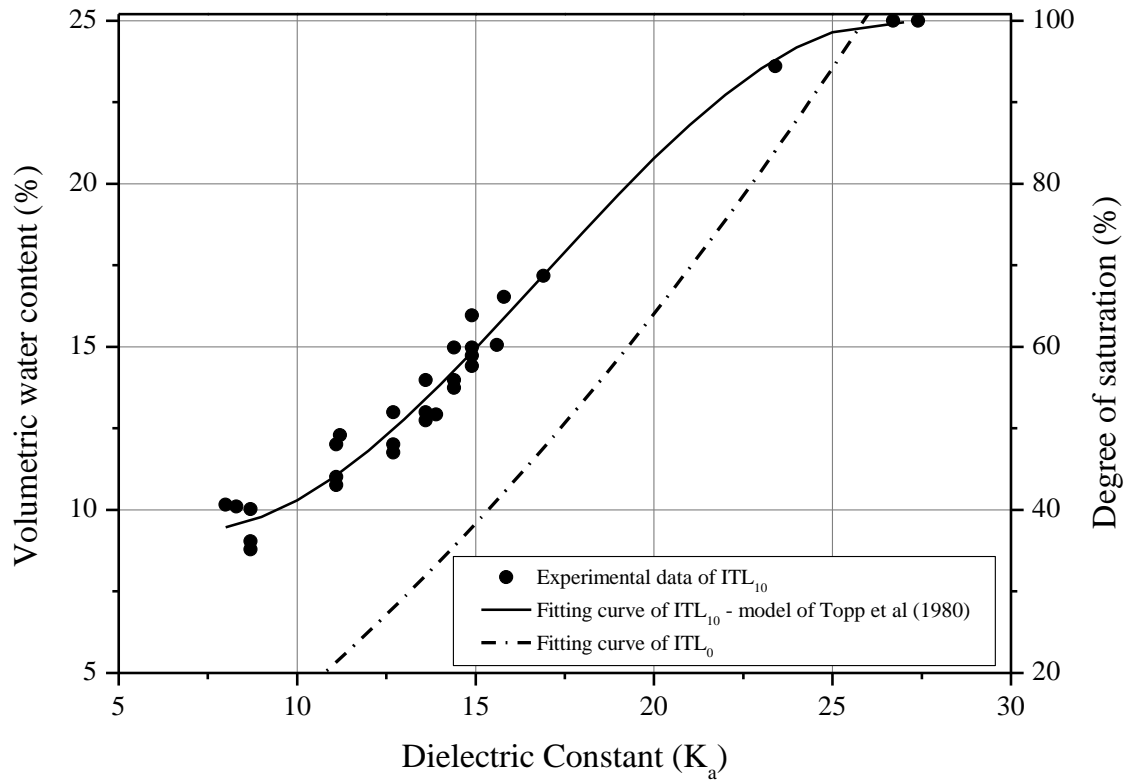
630  
631

Fig. 1: Grain size distribution curves of the interlayer soil ( $ITL_0$ ) and the derived ones ( $ITL_{10}$  and Fines)



632

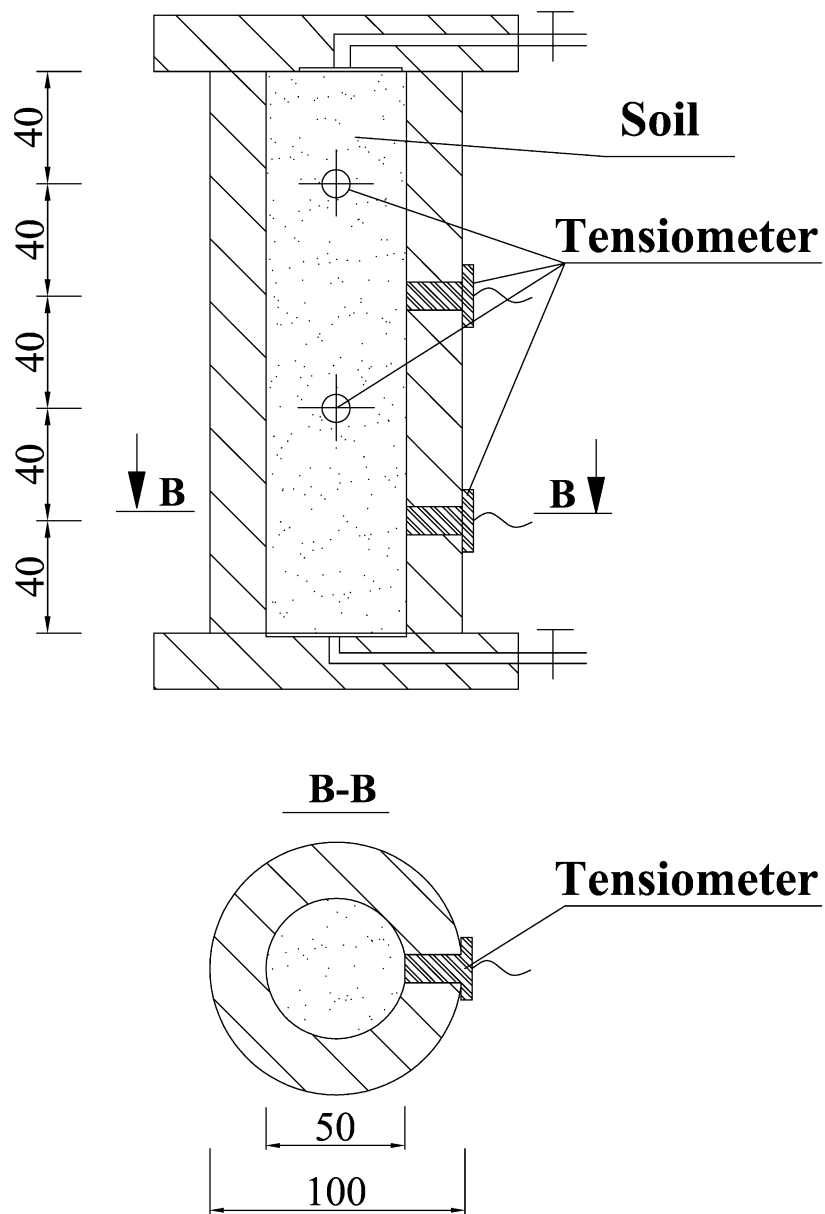
633 Fig. 2: Schematic view of the large-scale infiltration column



634

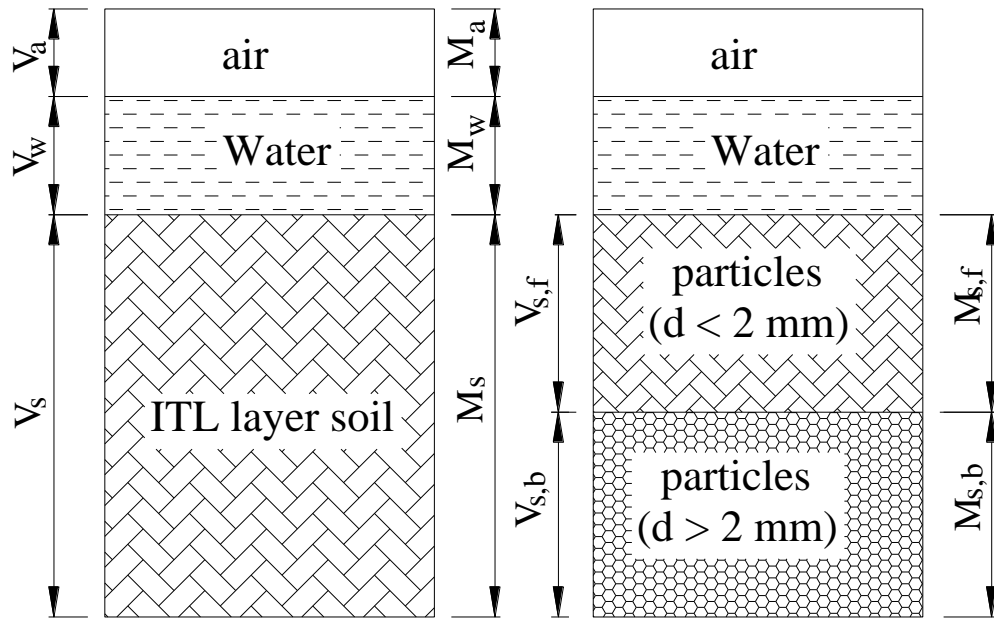
635 **Fig. 3: Calibration curves of the TDRs used for the  $ITL_{10}$  and  $ITL_0$  specimens**

636



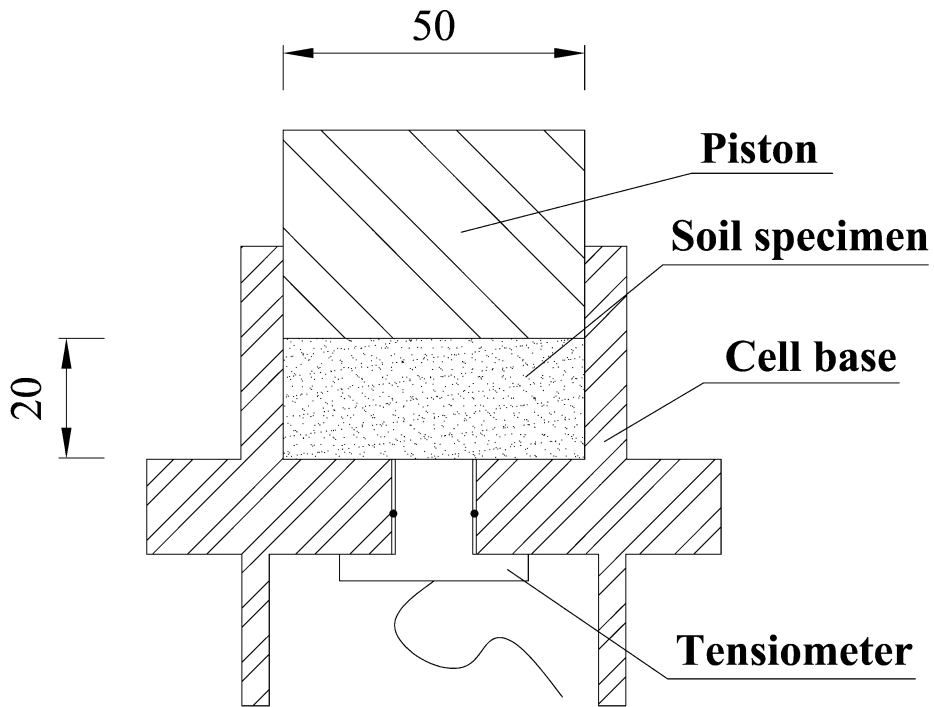
637

638 Fig. 4: Schematic view of the small-scale infiltration column



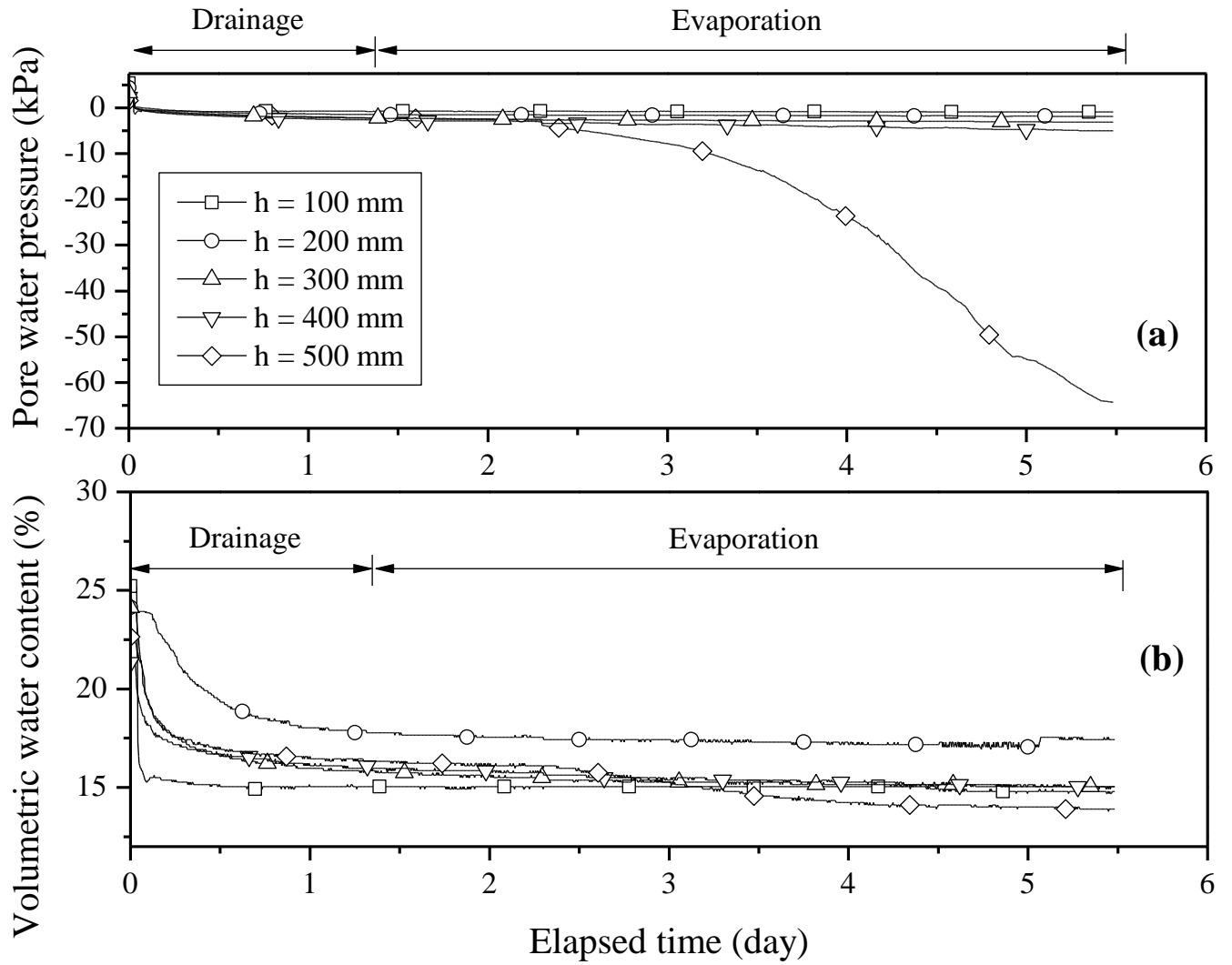
639

640 **Fig. 5: Components of the unsaturated interlayer soil**



641

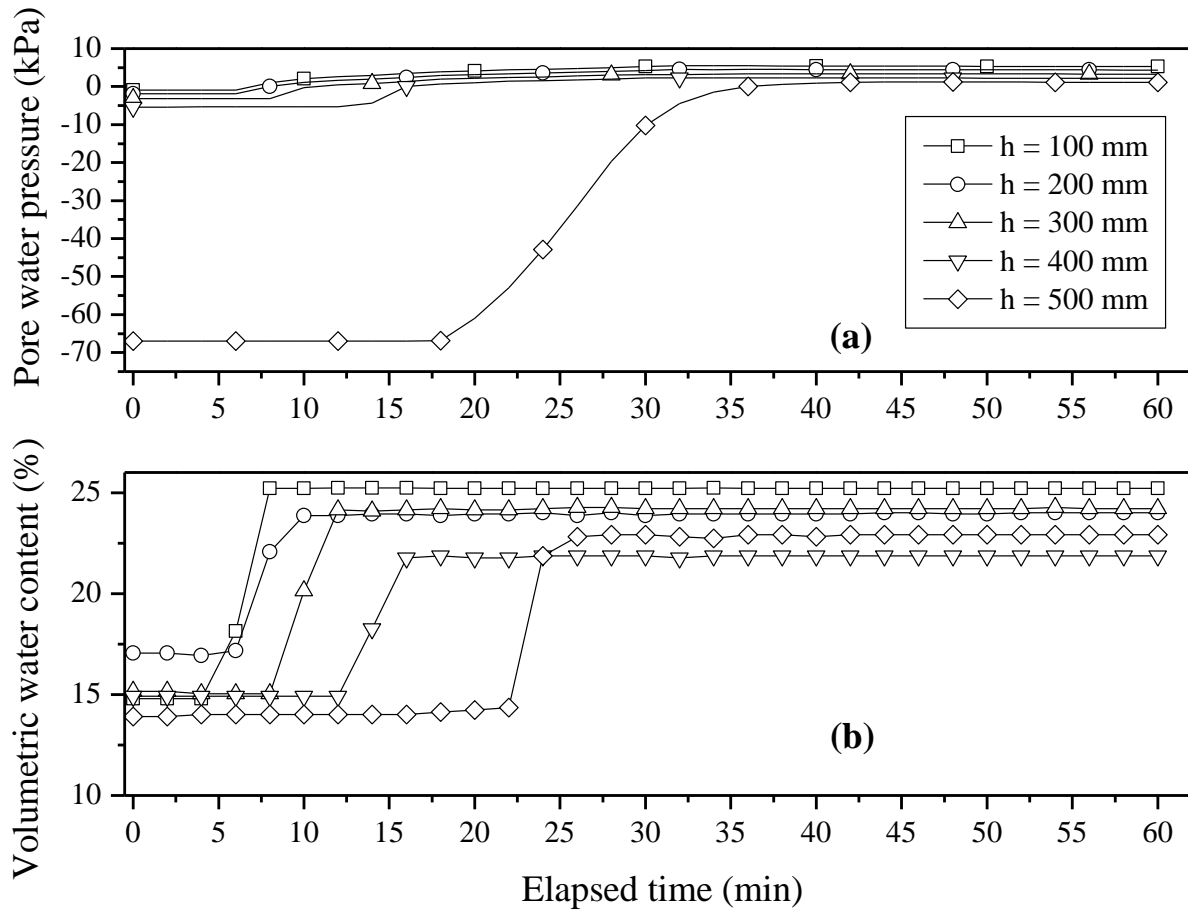
642 **Fig. 6: Device for determining the WRC of Fines**



643

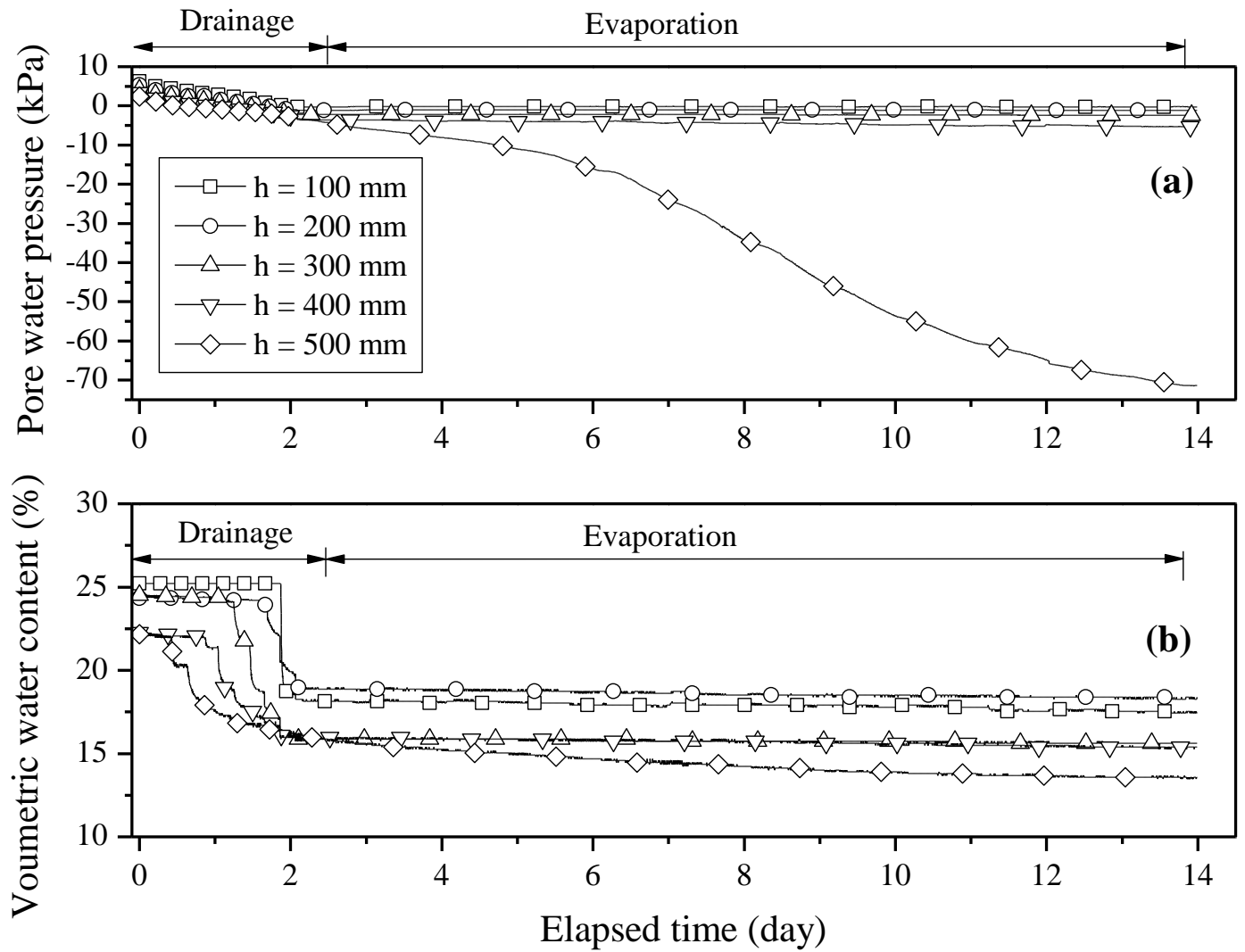
644 Fig. 7: Test on  $ITL_{10}$ : pore water pressure and volumetric water content evolutions during Drainage 1 and  
 645 Evaporation 1

646



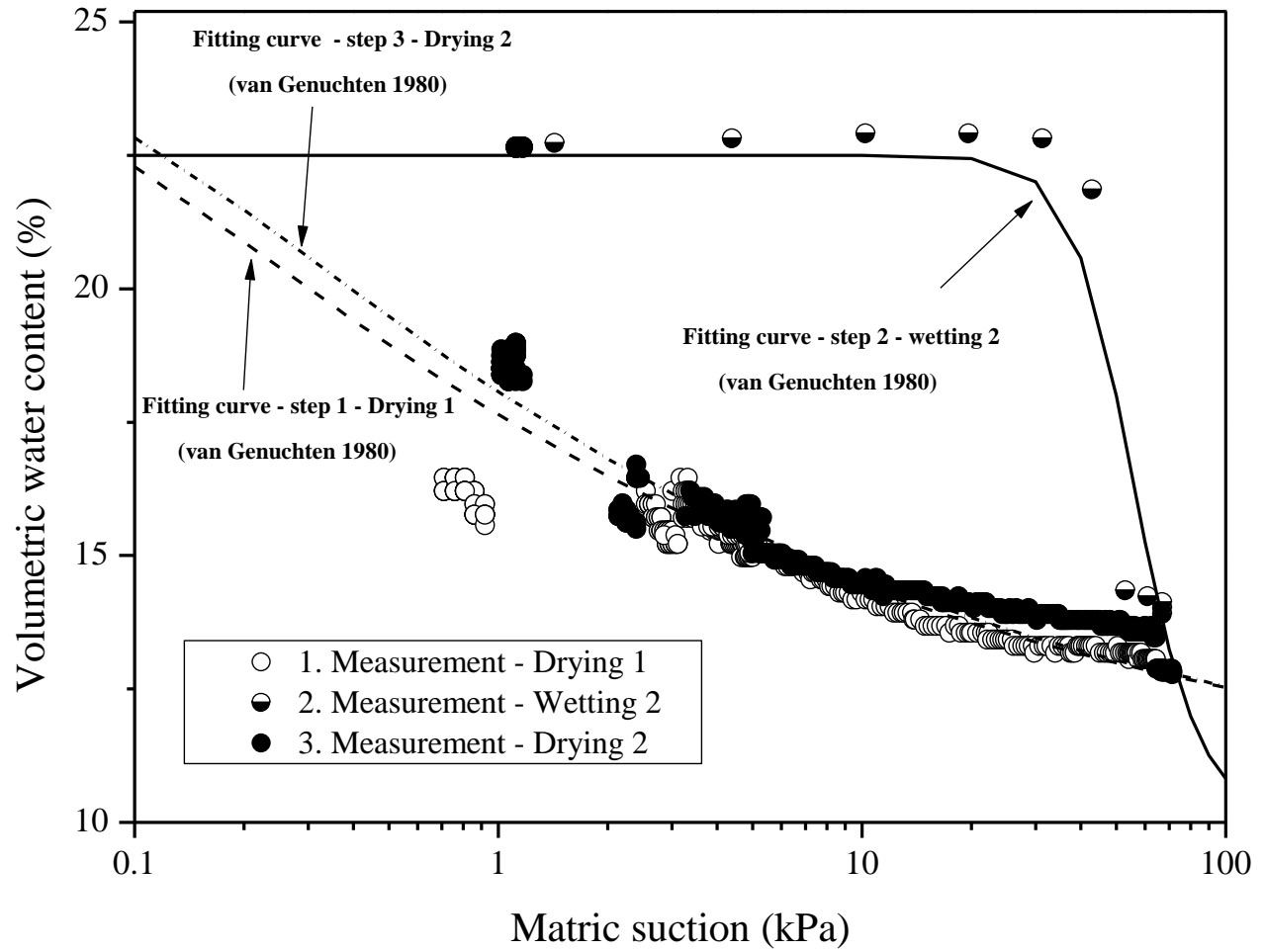
647

648 Fig. 8: Test on  $ITL_{10}$ : pore water pressure and volumetric water content evolutions in Saturation 2



649

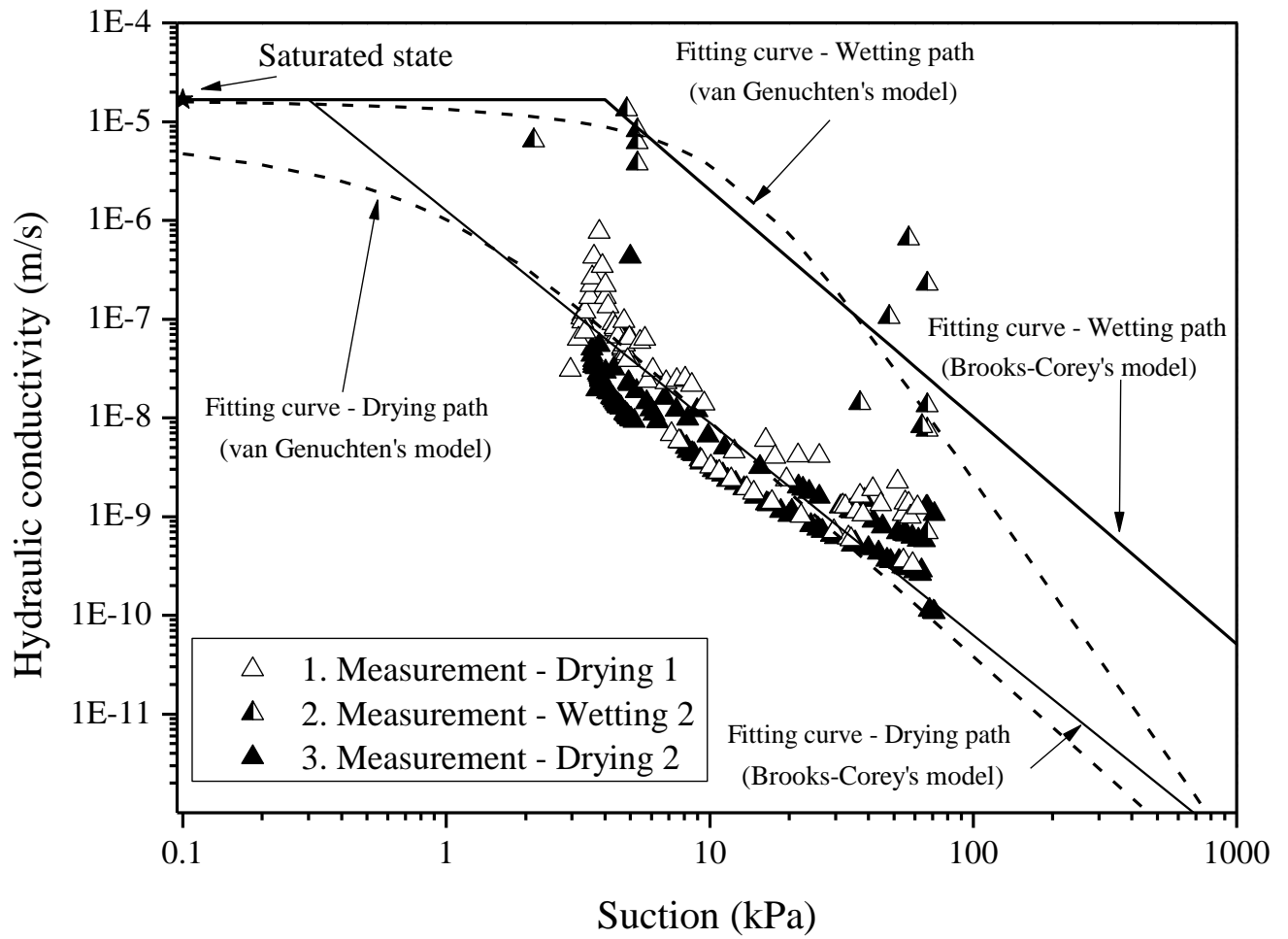
650 Fig. 9: Test on *ITL*<sub>10</sub>: pore water pressure and volumetric water content evolutions during Drainage 2 and  
 651 Evaporation 2



652

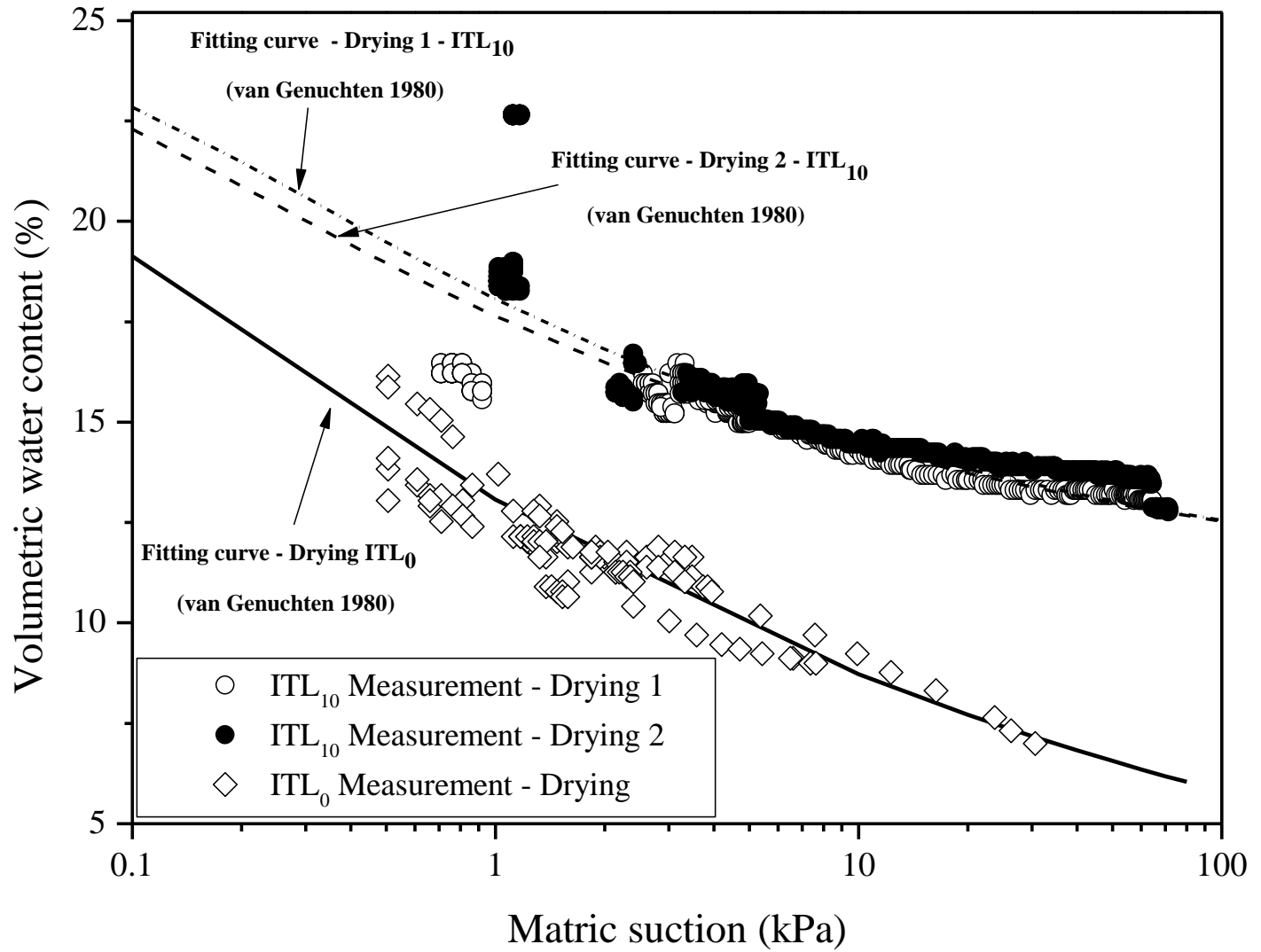
653 Fig. 10: WRC of  $ITL_{10}$  with fitting curves using the van Genuchten's model (1980)

654



655

656 Fig. 11: Hydraulic conductivity of  $ITL_{10}$  obtained with drying-wetting cycles

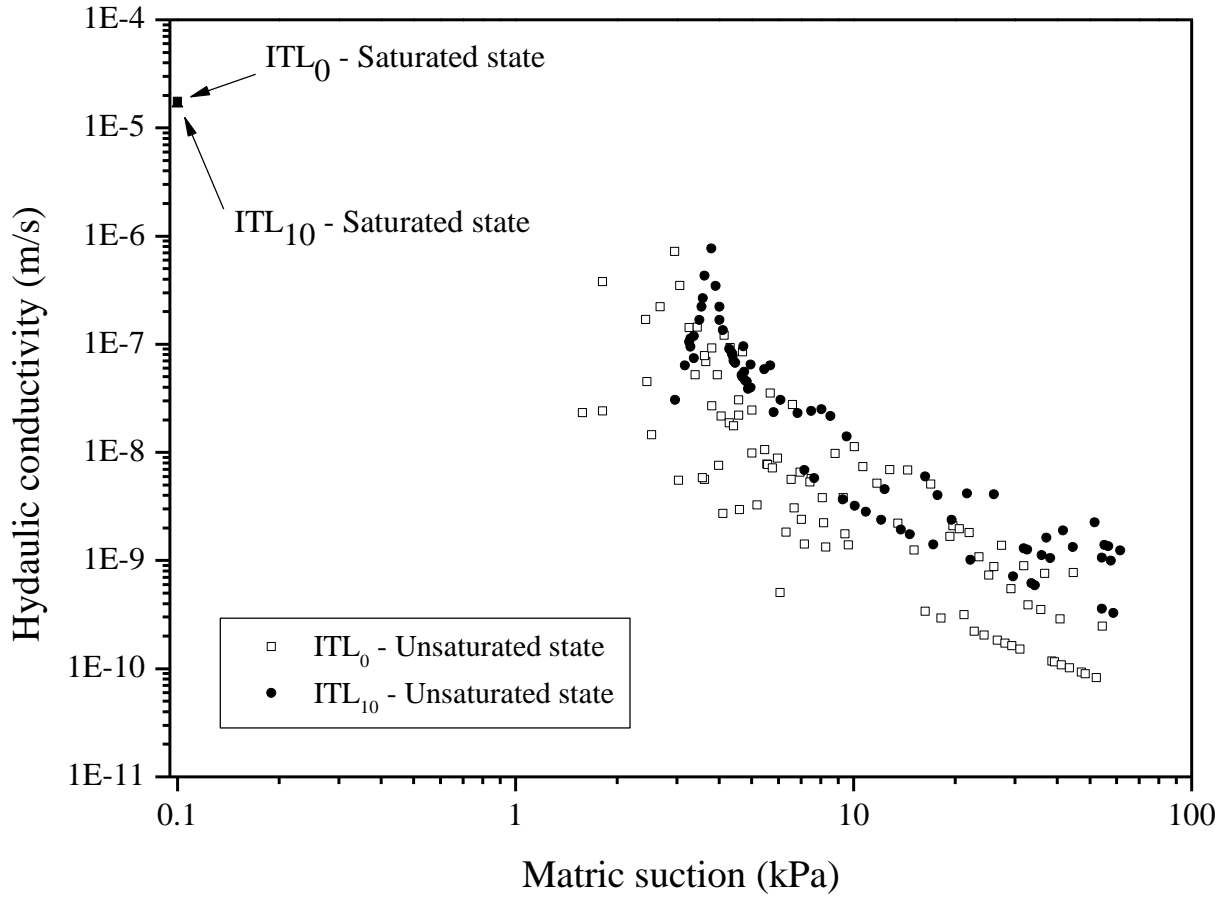


657

658 Fig. 12: Comparison of SWRC between  $ITL_0$  and  $ITL_{10}$

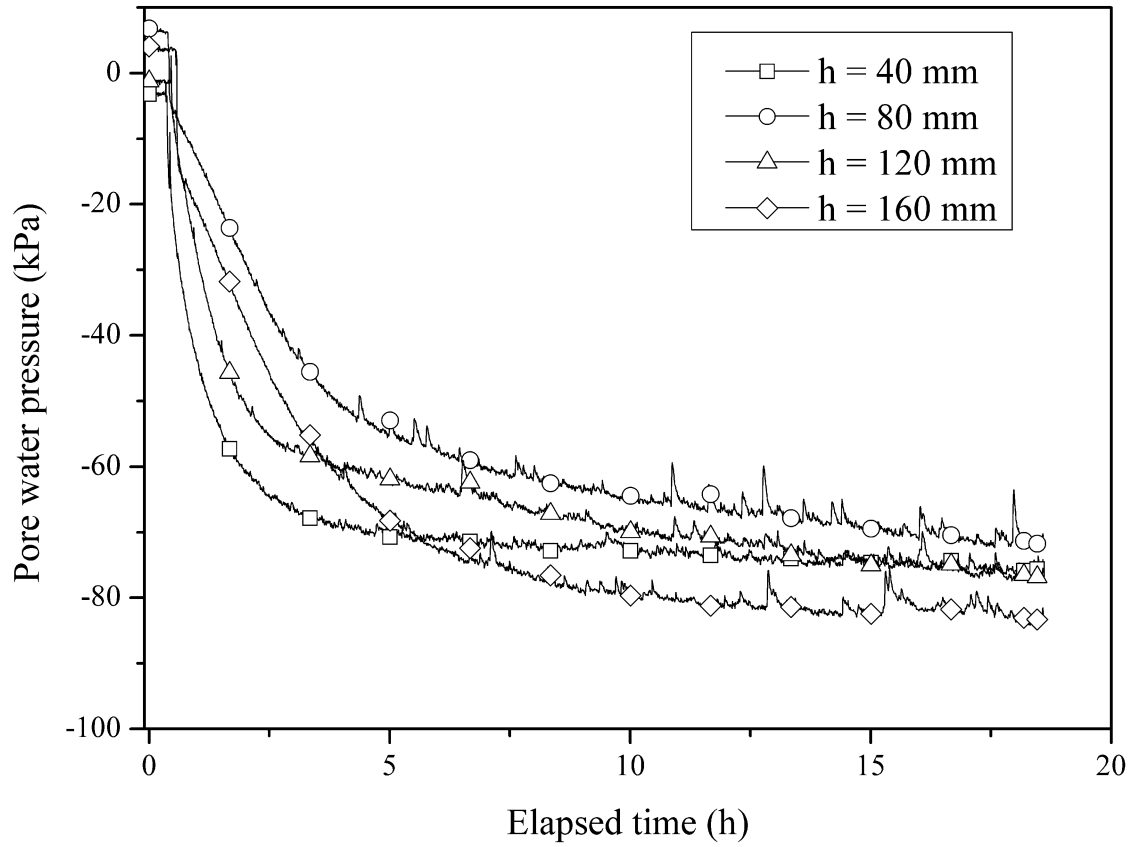
659

660



661

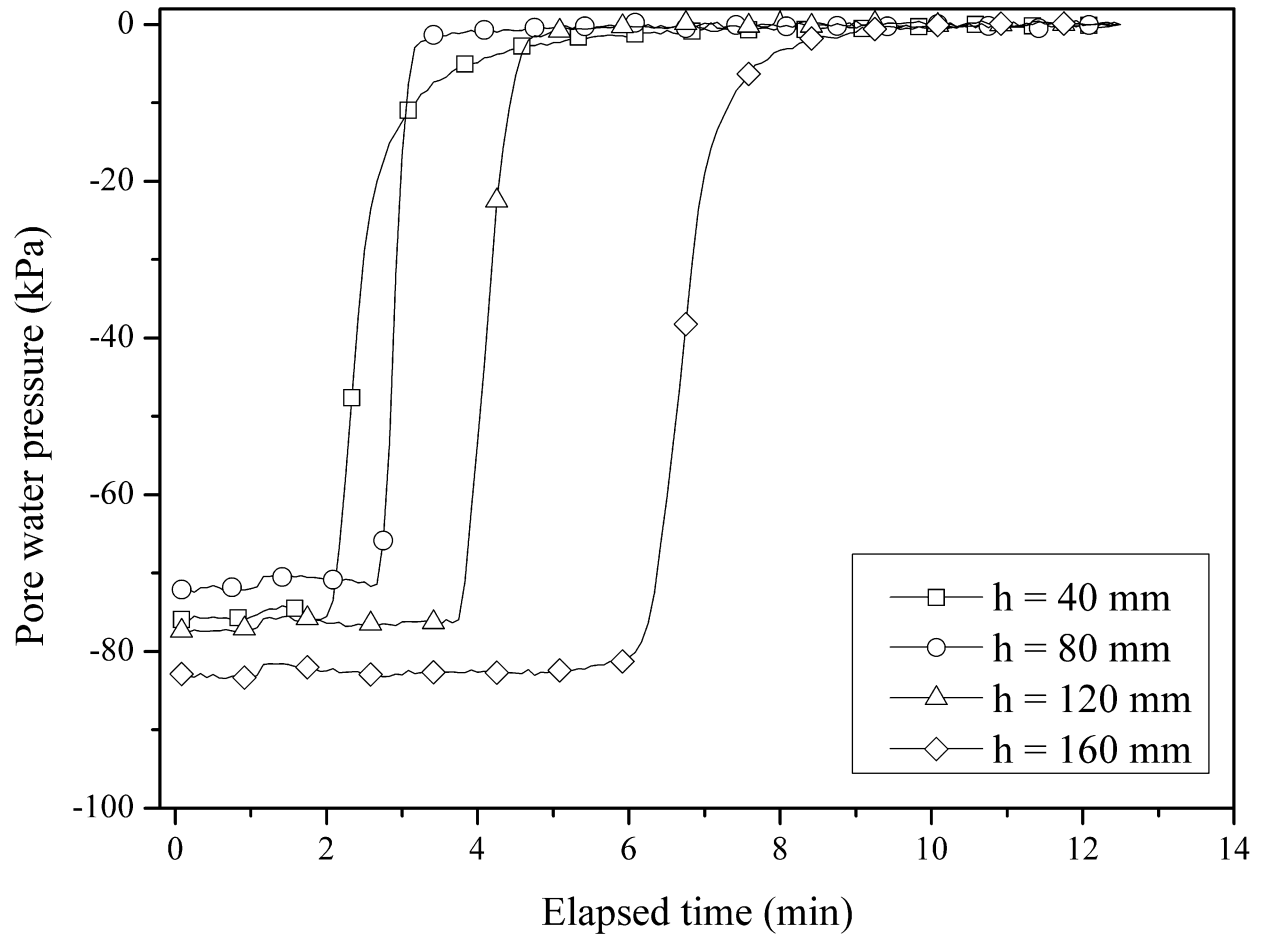
662 Fig. 13: Comparison of hydraulic conductivity between  $ITL_0$  and  $ITL_{10}$



663

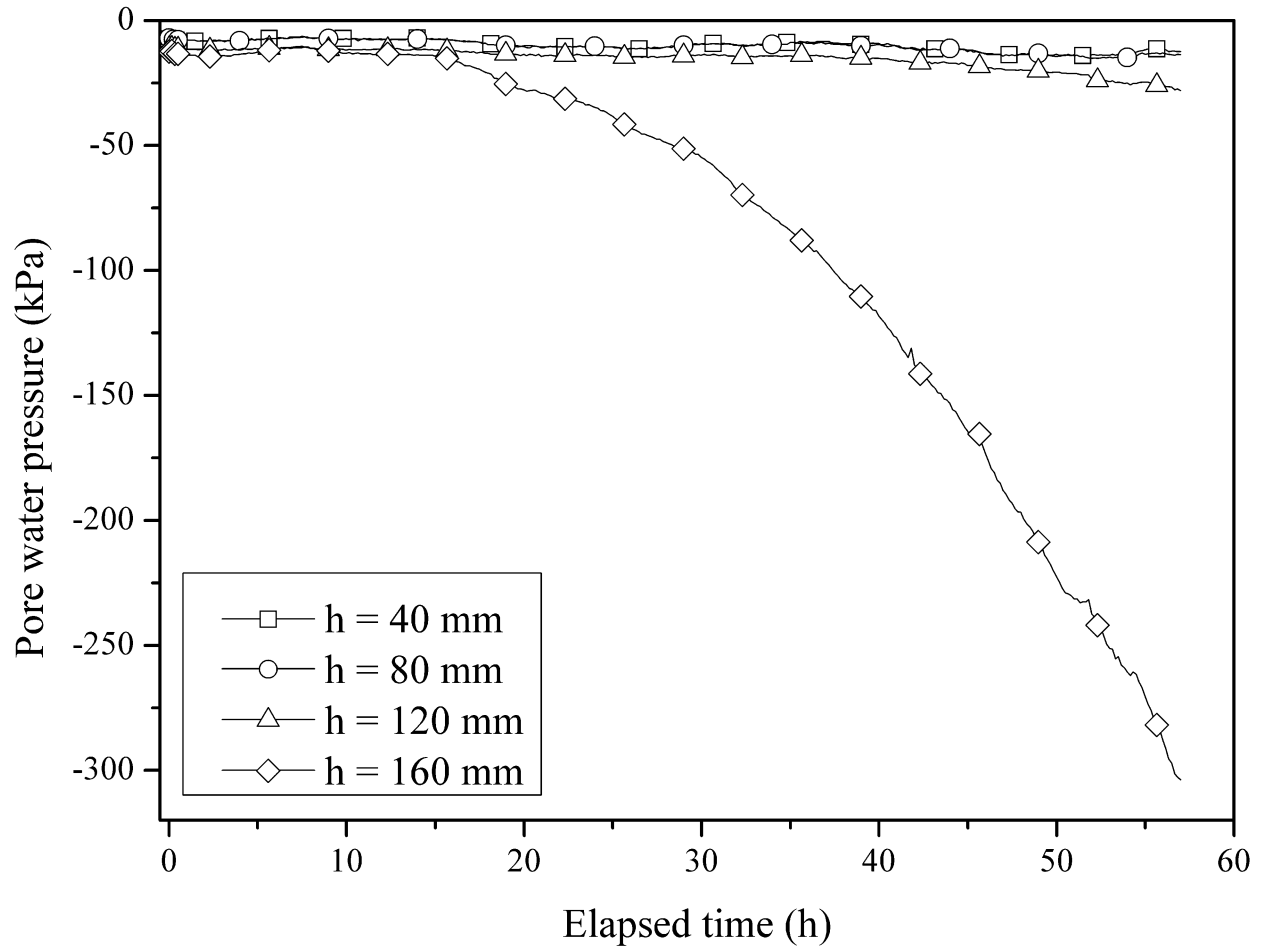
664 **Fig. 14: Test on *Fines*: suction stabilization after the installation of tensiometers**

665



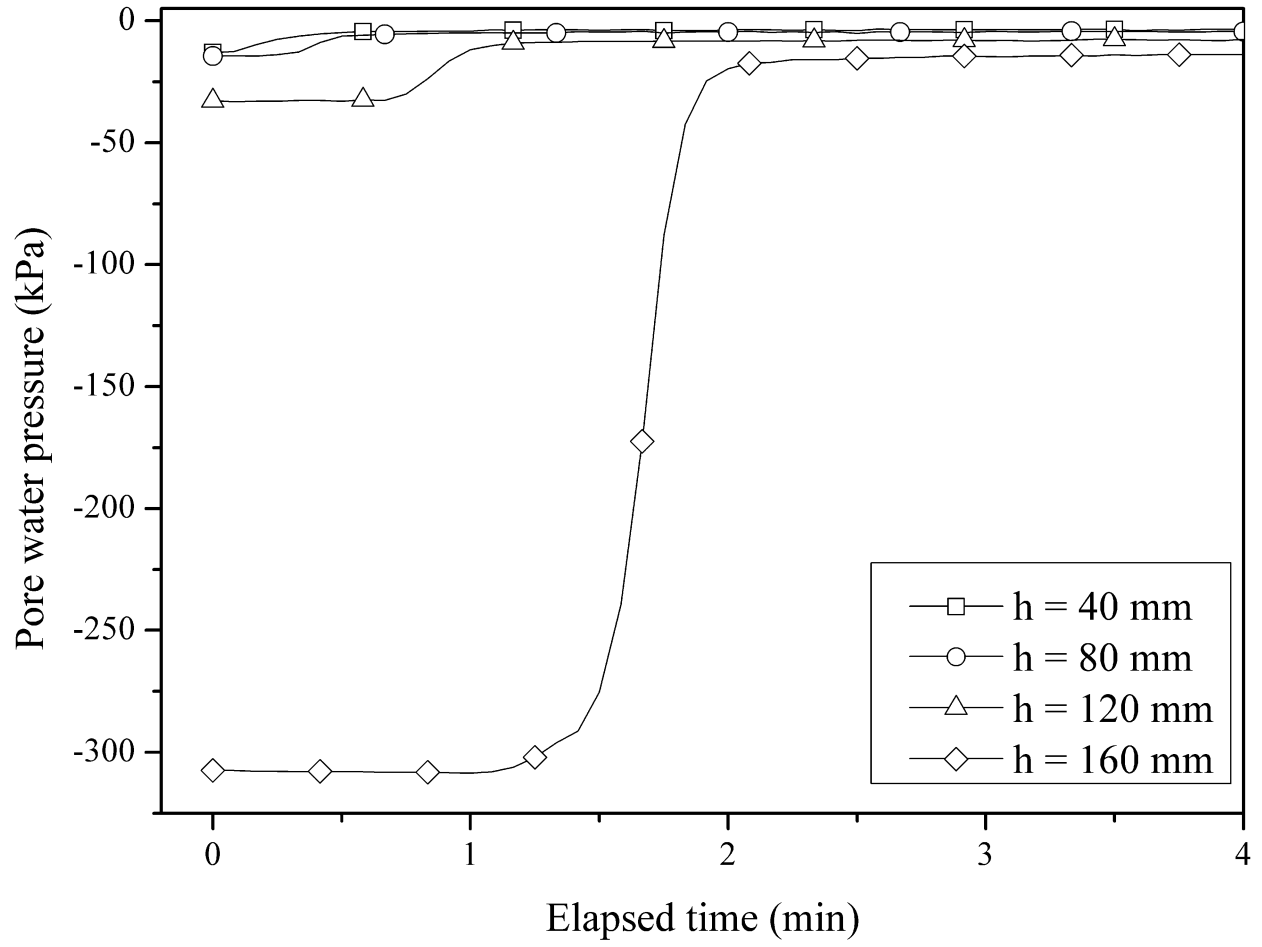
666

667 Fig. 15: Test on *Fines*: suction evolutions during Saturation 1



668

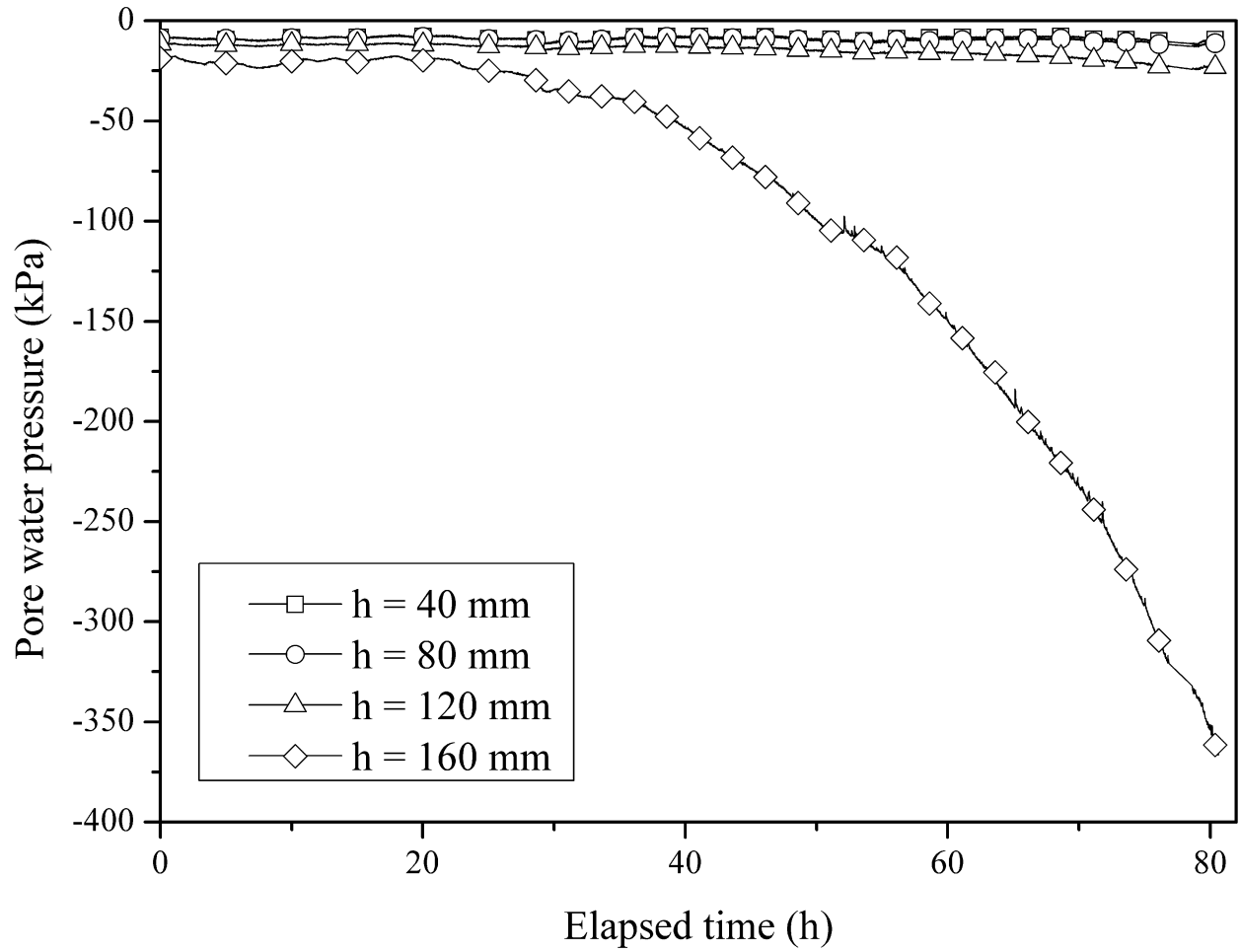
669 **Fig. 16: Test on *Fines*: suction evolutions during Evaporation 1**



670

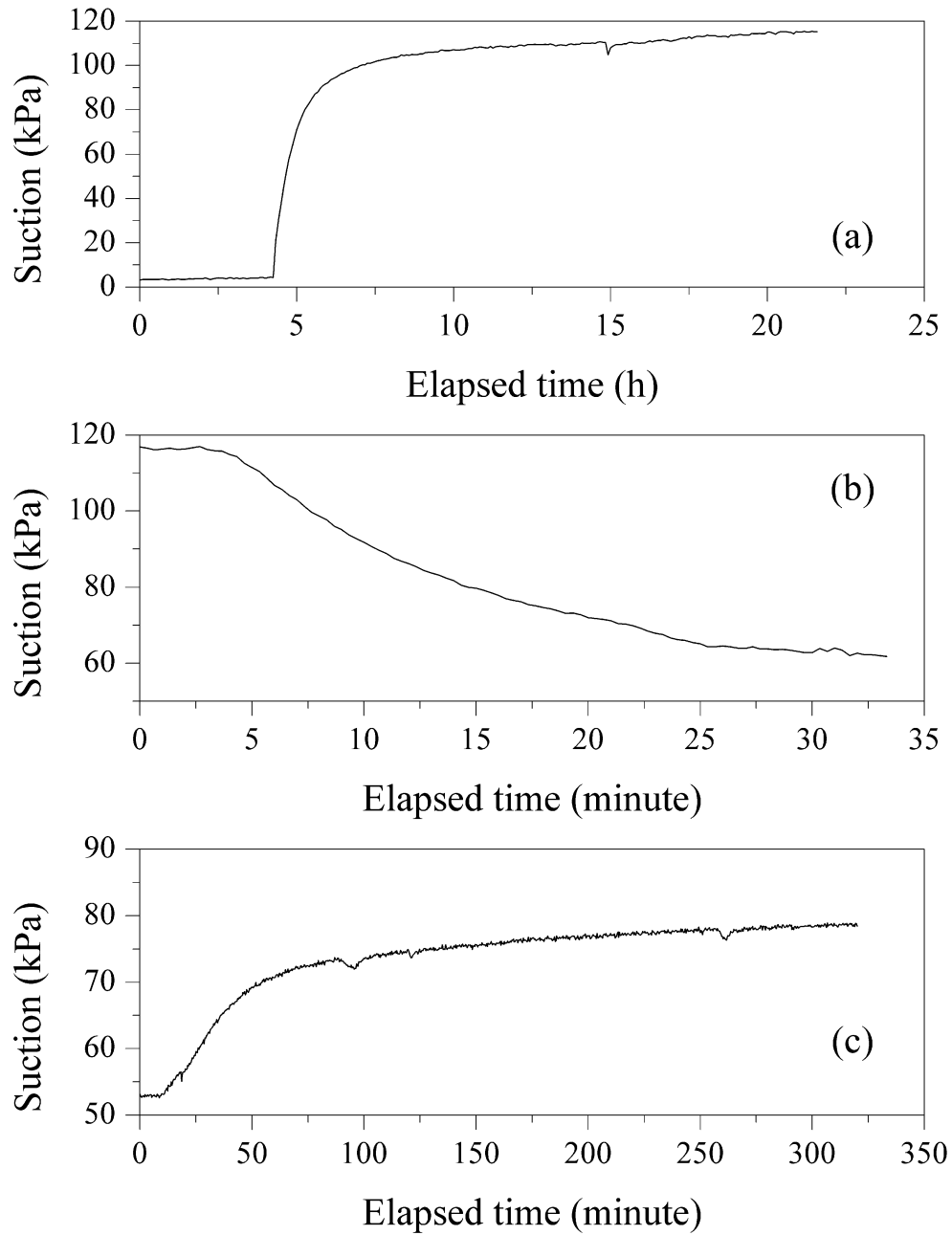
671 **Fig. 17: Test on *Fines*: suction evolutions during Saturation 2**

672



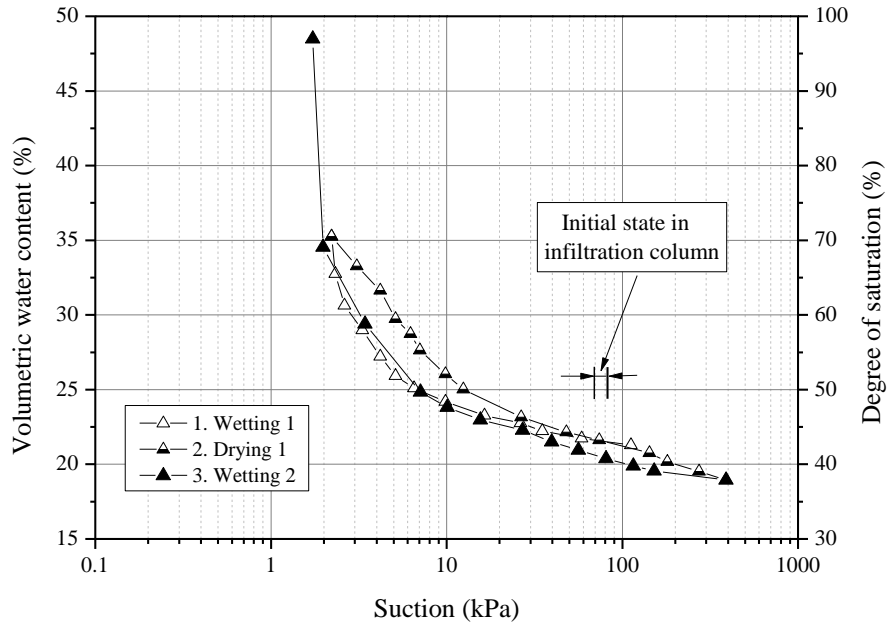
673

674 Fig. 18: Test on *Fines*: suction evolutions during Evaporation 2



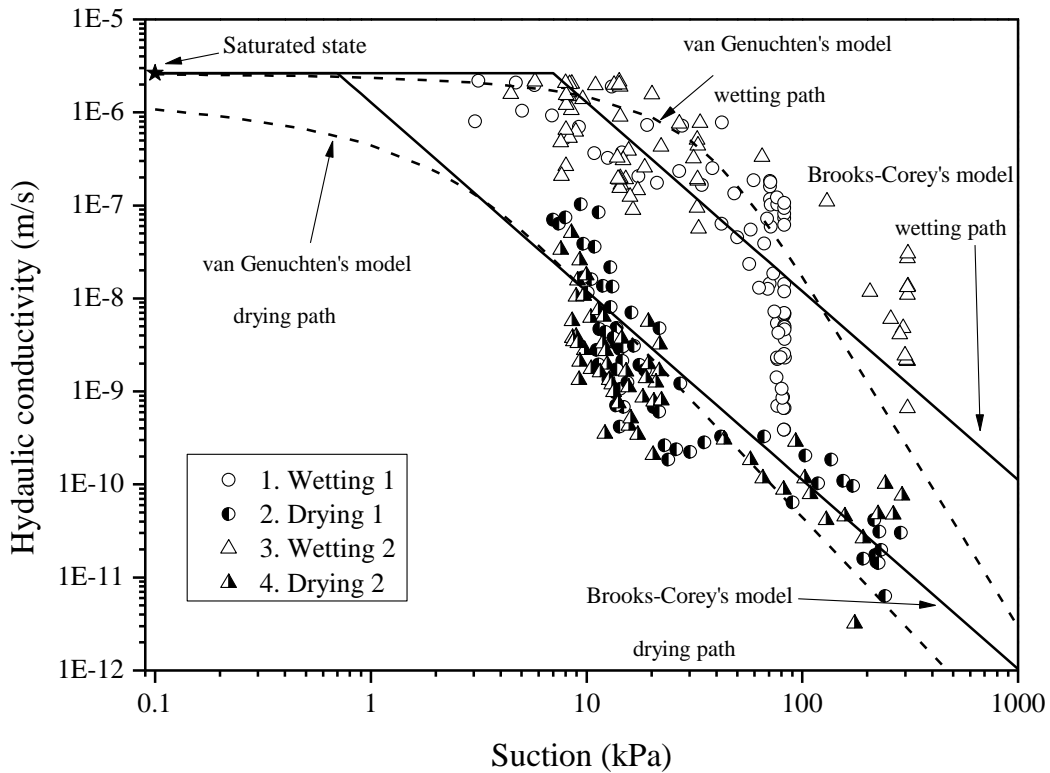
675

676 **Fig. 19: Stabilization of suction during the SWRC determination. (a) initial stabilization after tensiometer**  
 677 **installation, (b) a wetting stage, (c) a drying stage**



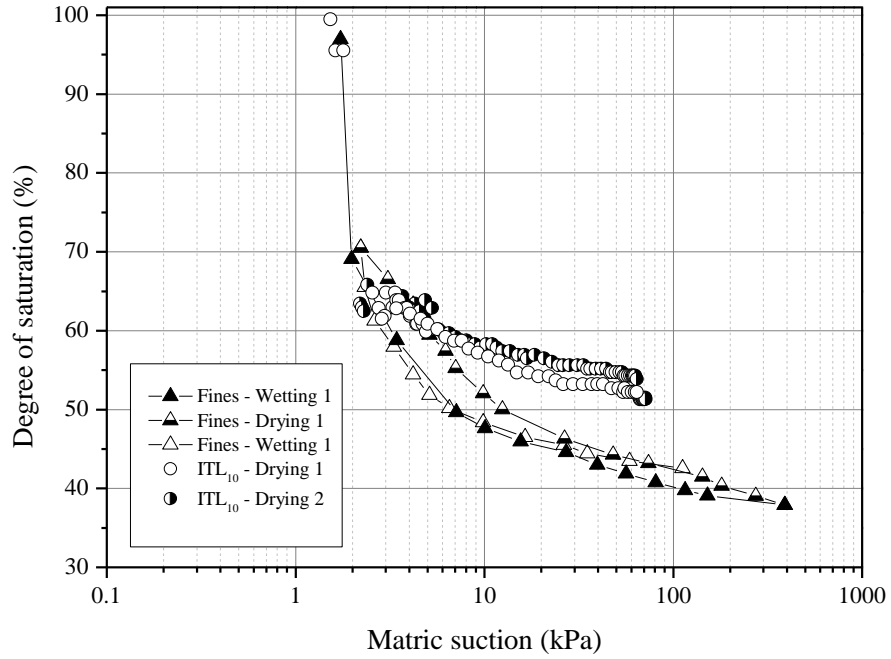
678

679 **Fig. 20: WRC of Fines**



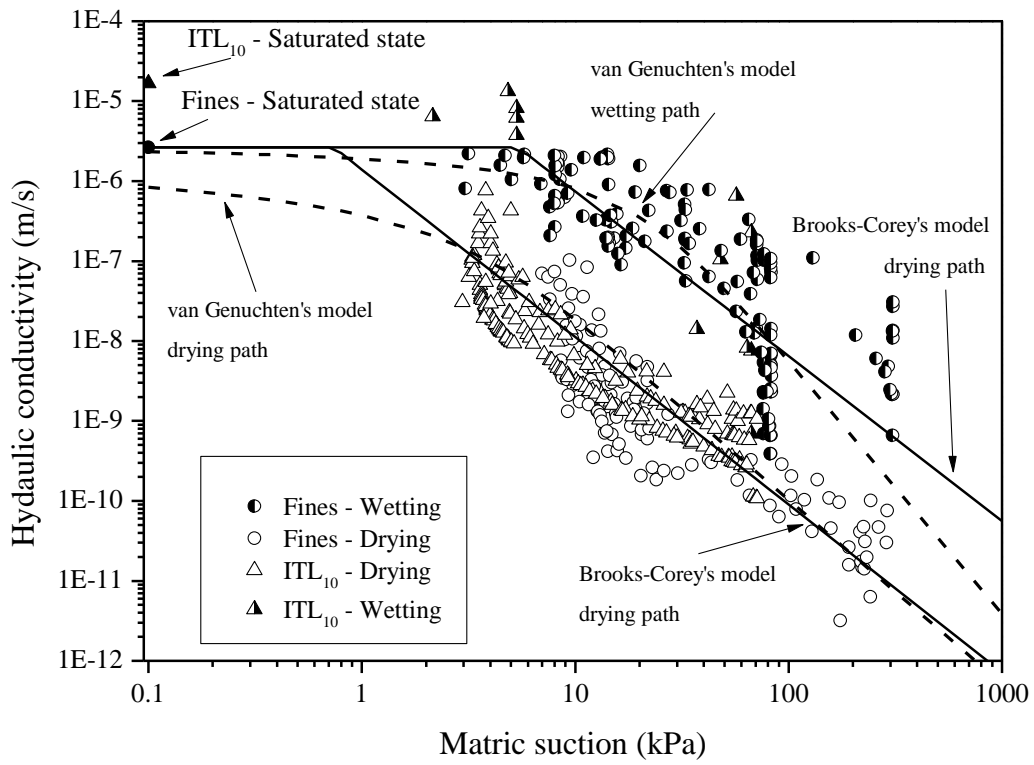
680

681 **Fig. 21: Hydraulic conductivity of Fines, obtained with drying/wetting cycles**



682

683 **Fig. 22: Comparison of SWRC between  $ITL_{10}$  and *Fines***



684

685 **Fig. 23: Comparison of hydraulic conductivity between  $ITL_{10}$  and *Fines***